Future heat extremes and impacts in a convection permitting climate ensemble over Germany

Marie Hundhausen[1], Hendrik Feldmann[1], Natalie Laube[1], and Joaquim G. Pinto[1]

[1]Institute of Meteorology and Climate Research, Department Tropospheric Research (IMK-TRO), Karlsruhe Institute of Technology (KIT), Karlsruhe, Germany

Correspondence: Marie Hundhausen (marie.hundhausen@kit.edu)

Abstract. Heat extremes and associated impacts are considered the most pressing issue for German regional governments with respect to climate adaptation. We explore the potential of an unique high-resolution convection permitting (2.8 km), multi-GCM ensemble with COSMO-CLM regional simulations (1971-2100) over Germany regarding heat extremes and related impacts. We find a systematically reduced cold bias especially in summer in the convection permitting simulations compared to the driving simulations with a grid size of 7 km and parametrized convection. The projected increase in temperature and its variance favors the development of longer and hotter heat waves, especially in late summer and early autumn. In a 2° (3°) warmer world, a 26 % (100 %) increase in the Heat Wave Magnitude Index is anticipated. Human heat stress (UTCI>32°C) and local-specific parameters tailored to climate adaptation, revealed a dependency on the major landscapes, resulting in significantly higher heat exposure in flat regions such as the Rhine Valley, accompanied by the strongest absolute increase. A non-linear, exponential increase is anticipated for parameters characterizing strong heat stress (UTCI>32°C, tropical nights, very hot days). Providing local-specific and tailored climate information, we demonstrate the potential of convection permitting simulations to facilitate improved impact studies and narrow the gap between climate modelling and stakeholder requirements for climate adaptation.

1 Introduction

The last two decades have been characterised by an increased number of summer heat waves (HWs), some of them of unprecedented magnitude and impact (e.g. Schär and Jendritzky, 2004; García-Herrera et al., 2010; Barriopedro et al., 2011; Russo et al., 2015). HWs are the most visible sign of ongoing global warming in Central Europe (IPCC, 2021), which lead to an increased awareness in our society and stakeholders (Lee et al., 2015; Moser, 2016). As a result, both government agencies and the private sector have not only developed plans for long-term investments towards climate protection but also for the development of sustainable adaptation strategies, which are now regularly finding their way into policy agenda (Biesbroek et al., 2010). In Germany, local governments are key actors implementing adaptation strategies (Hackenbruch et al., 2016). Nearly one fourth of the German cities had climate adaptation plans in place by 2018 (Reckien et al., 2018), documenting an increasing interest in the subject. Moreover, the German federal government has launched large research activities like the RegIKlim consortium (regional information for action on climate change) to further strengthen this development.

From the perspective of administrations in municipalities in Southern Germany, the greatest need for action lies indeed in the adapting to heat extremes (Hackenbruch et al., 2017). HWs – increased temperature over several consecutive days – are a threat to ecosystems, economy and human health (e.g. Basu and Samet, 2002; Poumadere et al., 2005). HWs are in fact the weather hazard causing the highest number of deaths in Europe (Zuo et al., 2015). E.g., for the European HW in 2003 alone, up to 80000 additional deaths were recorded over twelve European countries concerned by excess mortality (Robine et al., 2007). However, there is no unified definition of a HW. Different thresholds for e.g. length and temperature can be found in the literature, and a variety of indices have been developed for classification, e.g. Warm Spell Duration Index (WSDI) (Alexander et al., 2006), Heat Wave Magnitude Index (HWMId) (Russo et al., 2014), or excess heat factor (EHF) (Nairn and Fawcett, 2015). Recent efforts have gone towards quantitative approaches and a higher comparability between methods (e.g. Perkins and Alexander, 2013; Russo et al., 2014; Becker et al., 2022), leading to a better understanding of the strengths, weaknesses and range of applicability of the individual indices. Irrespective of the index used, there is a clear consensus in the scientific community (IPCC, 2021) that HWs will become more severe in terms of duration, frequency and magnitude with increasing global warming, also in Central Europe.

Climate information on the regional to local scale is needed for the development of tailored climate adaptation measures. This can be achieved with regional climate models (RCM), which perform a downscaling of the climate projections from global climate models (GCMs) to the required spatial and time scales, as it is done in the Coordinated Regional Downscaling Experiment CORDEX (e.g. Jacob et al., 2014). Novel developments include RCM simulations performed with a grid spacing under 4 km, which resolves convection permitting scales and thus parametrizations of deep convection are not required (convection permitting models, CPM) (Prein et al., 2015). Due to the very high resolution on the scale of urban districts, relevant data fields can be either derived directly or allow a direct coupling with impact models. Several recent studies have documented the advantages of these convection permitting simulations, both in terms of dominant convective precipitation and regions with strong spatial heterogeneity as present in mountainous or urban areas (Prein et al., 2015). Regarding the representation of temperature, there is not yet a consensus on added value in convection permitting simulations. Whereas Prein et al. (2013) and Brisson et al. (2016) attribute improvements of the temperature output to the better resolution of orography, Ban et al. (2014) even found an increasing bias on the convection permitting scale but improvements of the diurnal cycle of temperature in a domain covering the alpine region. In contrast, an improvement of mean temperature was found in Hohenegger et al. (2008) for most of her study area and in investigations by Hackenbruch et al. (2016) over Germany. In addition, Tölle et al. (2018) found an added value for temperature extremes. Mixed results with a regional dependency were found in Soares et al. (2022), concluding a gain for temperature due to an improved spatial representation of local atmospheric circulations and land-atmosphere interactions.

To quantify the associated uncertainties of the regional climate projections, ensemble simulations are required. As the computational costs in CPM are (very) high, many climate studies are based on single model projections, and only few studies using CPM ensembles exist (Prein et al., 2015). Very first ensembles of convection permitting climate projections exist e.g. from the CORDEX Flagship Pilot Study on Convection (FPSConv; Pichelli et al. (2021); Ban et al. (2021)). There, several GCMs from the Coupled Model Intercomparison Project CMIP5 (Taylor et al., 2012) using the RCP8.5 scenario (Van Vuuren et al., 2011) were downscaled by multiple RCMs to a common grid with 3 km resolution covering the larger Alpine area (ALP-3). They used

10-year time-slices for the historical period (1996-2005) and two future periods (2041-2050 and 2090-2099). The current study applies a different ensemble approach, that is a four-member ensemble of convection permitting climate projections performed by a single RCM, downscaling four GCMs under the scenario RCP8.5. All simulations cover the period from 1971 to 2100 in a quasi-transient manner, where the projection is composed of several time slices. To our best knowledge, an ensemble of this temporal extent is currently unique. Such a long simulation period allows for a better statistical representation of extremes and the application of approaches used for typical coarser scale transient GCM or RCM ensembles, like e.g. the analysis for different Global Warming Levels (GWL) as it is used in the IPCC AR6 (Lee et al., 2021) to compare climate change signals for GCMs with different climate sensitivity or between different emission scenarios.

Our focus in this study is heat extremes and related impacts under global warming compared to recent climate conditions. Specifically, we were motivated by three guiding questions:

1. What are the benefits of convection permitting models for temperature extremes in Germany? (Section 3)

2. What can we learn from a convection permitting ensemble about future regional temperature trends and HW characteristics? (Section 4 & 5)

3. What is the impact of these changes on heat stress and other regionally mapped tailored climate parameters? (Section 6)

The paper is structured as follows: Section 2 describes the methodology and the used datasets. Section 3, 4, 5, and 6 focus on the results guided by the three research questions, while a summary and discussion conclude the paper in section 7.

2   Data and method

2.1   The COSMO-CLM ensemble

The simulations analysed in this study have been generated in the context of the projects KLIWA (Klimaveränderungen und Konsequenzen für die Wasserwirtschaft) and extended within the project ISAP (Integrative urban-regional adaptation strategies in a polycentric growth region: Model region – Stuttgart Region). The regional climate simulations are conducted using the RCM COSMO5.0-CLM9 (CCLM, Rockel et al. (2008)). CCLM originates from the German weather service forecast model COSMO (Baldauf et al., 2011), which is a three-dimensional, non-hydrostatic, fully compressible numerical model for the atmosphere including a multi-layer soil-vegetation transfer model TERRA-ML (Schrodin and Heise, 2001). The RCM has been applied for multiple studies over different CORDEX domains (Sørland et al., 2021) and on the kilometre-scale within the CORDEX Flagship Pilot Study on convection (Ban et al., 2021; Pichelli et al., 2021).

Initial and boundary data are provided by four GCMs (cf. Table 1) from the CMIP5 generation under the scenario RCP8.5 (Van Vuuren et al., 2011). The selected GCMs cover a wide range of climate sensitivities (Nijsse et al., 2020), that is parametrized over the equilibrium climate sensitivity (ECS) – the global mean surface air temperature increase that results from a doubling of atmospheric CO_2 (Table 1). In addition, an evaluation simulation, downscaling ERA40 (Uppala et al., 2005) over the period 1971-2000 is included (Hackenbruch et al., 2016), using the same setup as the projections.

The ensemble was generated in a three-step nesting approach (Table 2; Fig. 1a) with a first nest over Europe with 0.44 ° grid resolution, an intermediate nest over Central Europa with 7 km resolution, and an inner nest that encompasses the area of Central/Southern Germany and the Alpine area with 2.8 km resolution. The convection for the first two nests is parametrized using the Tiedtke-scheme (Tiedtke, 1989). For the innermost domain, this parametrization is only used for shallow convection as in Hackenbruch et al. (2016). In the current setup, the boundary zone between the inner nests is relatively narrow. However, we can benefit from a relatively small horizontal resolution step (less than a factor of 3) between the nests, which is smaller than common convection permitting setups used today (Ban et al., 2021). This is likely to decrease boundary effects and enable a tighter nesting. Nevertheless, the boundary zone that was excluded for the analysis of the innermost domain was considerably large (48 grid points, 137 km). Our examination of the results revealed that anomalies of temperature, as well as mean and extreme precipitation, occur well outside the evaluation area. The first two nesting levels were performed in a transient way. The third nest was originally performed in 30-year time-slices preceded by a three year spin-up (1968-2000; 2018-2050; 2068-2100; Schädler et al. (2018)). These time-slices were later on extended (2001-2020; 2051-2070) to provide a quasi-transient ensemble for the whole period. The overlapping periods (2018-2020 and 2068-2070) were compared (not shown). No relevant differences were found several months after simulation start, in accordance with the findings from Lavin-Gullon et al. (2022).

This continuous time-series data enabled us to apply the concept of Global Warming Levels (GWLs) (Lee et al., 2021), allowing an improved comparability from the downscaling of GCMs with differing climate sensitivities or different emission scenarios. Therefore, this approach mitigates parts of the GCM and scenario uncertainties and provides more specific information about the effects of climate change given a certain threshold of warming. Specifically, we analyse the +2 K and +3 K GWLs, which was possible for all GCMs due to the use of the high-end scenario RCP8.5. An overview of the simulations is given in Table 1. The period 1971-2000 is used as a historical reference period, which is attributed a global warming of 0.46 K. Table 1 lists the 30-year periods for the GCMs, which are centered around the respective year of the threshold exceedance similar to Teichmann et al. (2018).

As a strong dependency of the temperature output on the major landscape was detected, the area is narrowed down to a geographically more homogeneous area (Fig. 1b), including the Central Uplands, the South German Scarplands and the Alpine Foreland. Therefore, the domain focuses on the hilly parts of Germany, excluding the flat regions in Northern Germany and the mountainous regions – the Alps – in the very south. This domain, later referred to evaluation area, is bordered in red in Fig. 1b and is used in this study when statistics are applied over several grid points. The analysis in the paper is largely focused on HWs and associated impacts in the warm season. Since we observed the largest changes in late summer and early fall, we limit the analysis in this case to the months of May through October. This period is referred to as the summer half-year below.

To evaluate the skill of the convection permitting simulation, a comparison of observation data with the second, convection parametrizing nest and the third, convection permitting nest is performed on the raw, uncorrected model output in Sec. 3. The HYRAS dataset is used as observation, which is based on station data that are aggregated to a gridded dataset using the REGNIE method of combining a regression model and inverse distance weighting (Rauthe et al., 2013; Razafimaharo et al., 2020). The comparison is conducted for the reference period 1971-2000 for the evaluation run driven by ERA40 as well as for all ensemble members. Simulation data were interpolated on the HYRAS grid with a grid spacing of 5 km. In addition, a height
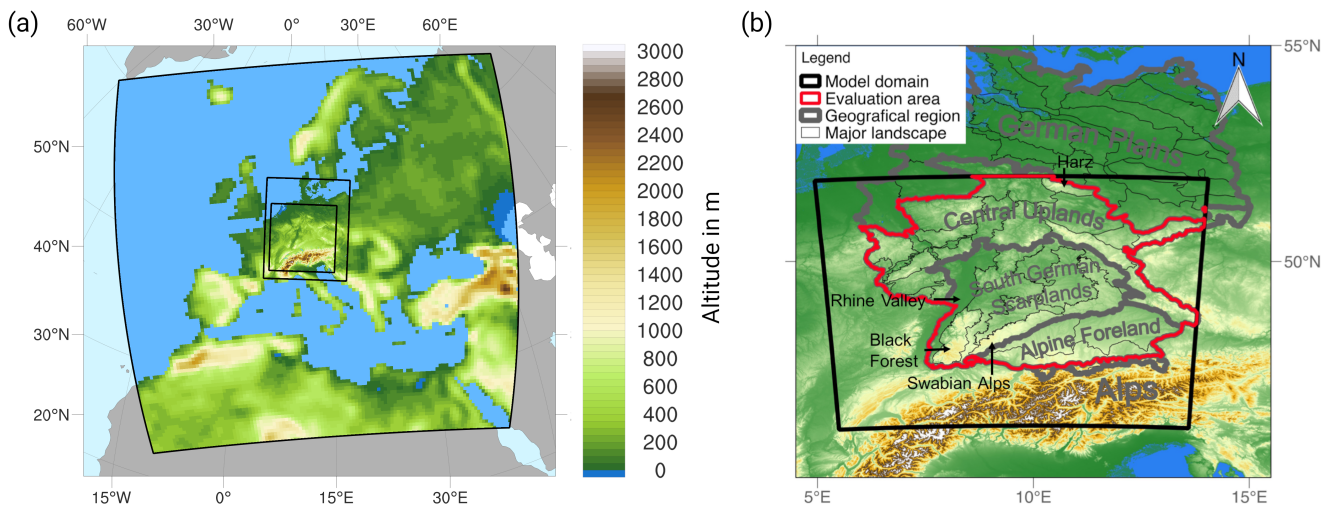
Figure 1. In (a) the three nesting levels are shown. (b) shows the model domain with the sponge area truncated and the used evaluation area in red. The borders of the German major landscapes were added in black. Important major landscapes for the evaluation are the Rhine Valley, the Black Forest, the Swabian Alps, and the Harz (Shapefiles of the major landscapes: Bundesamt für Naturschutz (BfN), 2015).

Table 1. Name, realization, Equilibrium Climate Sensitivity (ECS; cf. Nijsse et al. (2020) supplementary), 30-year periods corresponding to GWL +2 and +3 degrees relative to pre-industrial conditions and main reference for the CMIP5 GCMs downscaled for the ensemble.

GCM	Realization	ECS in °C	GWL2	GWL3	Reference
CNRM-CM5	r1i1p1	3.28	2029 - 2058	2052 - 2081	Voldoire et al. (2013)
MPI-ESM-LR	r1i1p1	3.66	2029 - 2058	2052 - 2081	Giorgetta et al. (2013)
EC-EARTH	r12i1p1	4.18	2026 - 2055	2051 - 2080	Prodhomme et al. (2016)
HadGEM2-ES	r1i1p1	4.64	2016 - 2045	2037 - 2066	Collins et al. (2011)

125 correction of temperature was applied along with the interpolation, assuming a vertical gradient of 0.0065 K/m. The correction compensates the effect of a height-dependent temperature that is favored by higher resolution of orography. The evaluation of the model skill was conducted prior to the bias correction.

2.2 Bias correction

In order to correct for a systematic error in climate simulations to obtain reliable data for impact assessment, it is common
130 practice to apply a bias correction (Maraun, 2016). Following the assumption that the model bias remains constant over time for each quantile of the model data, we apply quantile delta mapping according to Cannon et al. (2015). Its application to a modeled variable $x_{\mathrm{mod,pred}}$ at time step t in the prediction period (pred) is based on its non-exceedance probability P_t,

Table 2. Model setup.

Nesting level	Grid spacing	Grid dimensions (lat, lon, level)	Remarks
1st nest	0.44°, 50 km	$118 \times 110 \times 40$	Convection parametrized (Tiedtke, 1989)
2nd nest	0.0625°, 7 km	$160 \times 200 \times 40$	Convection parametrized (Tiedtke, 1989)
3rd nest	0.025°, 2.8 km	$322 \times 328 \times 49$	Only shallow convection parametrized

which is evaluated over the cumulative distribution function F (Eq. (1)). A quantile mapping of the value with the same non-exceedance probability P_t in the historical period (hist) is performed based on observed reference data (obs). To preserve the relative changes between the historical and the prediction period, the climate change signal Δ_m of the corresponding quantile is multiplied to obtain the corrected value $y_{\mathrm{mod,pred}}$ (Eq. (2) and (3)).

$$P_t = F_{\mathrm{mod,pred}}(x_{\mathrm{mod,pred}}(t)) \tag{1}$$

$$\Delta_m(t) = \frac{x_{\mathrm{mod,pred}}(t)}{F_{\mathrm{mod,hist}}^{-1}(P_t)} \tag{2}$$

$$y_{\mathrm{mod,pred}}(t) = F_{\mathrm{obs,hist}}^{-1}(P_t) \cdot \Delta_m(t) \tag{3}$$

A normal distribution was fitted to the distribution of absolute temperature to derive the transfer function. For the correction of precipitation, the empirical approach is used in contrast, as no added value was found with the distribution-based method using e.g. a gamma distribution. In addition, a dry-day correction following Ehmele et al. (2022) was applied prior to the correction for precipitation.

The bias correction was derived for the parameters daily mean temperature T_{mean}, daily minimum temperature T_{min}, daily maximum temperature T_{max}, and the daily precipitation sum P_{sum}. As reference, the observation dataset HYRAS with a resolution of 5 km was used, that was interpolated to the model grid. Along with the interpolation, a height correction of T_{mean}, T_{min} and T_{max} was applied assuming a vertical gradient of 0.0065 K/m. The available 30 years of the historical time slice from 1971 to 2000 were used as a reference period. To account for seasonal dependencies as discussed in Pierce et al. (2015), evaluation was done over a three month window. To minimize discontinuities at the edges of the time window (Pierce et al., 2015), the bias correction was applied for each month i of the year separately, using a transfer function derived and applied over month $i-1$ to month $i+1$.

This approach was chosen because it preserves the climate change signal of the quantiles, which is important for the relative description of heat waves used in the study. Furthermore, the method allows an application of the correction in a future climate
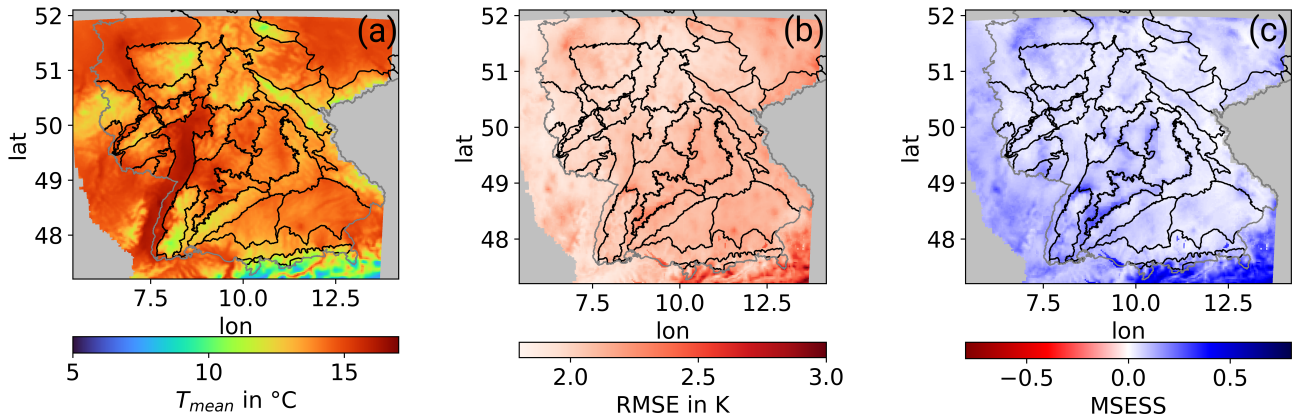
Figure 2. Impact of the bias correction of T_{mean} in the summer half-year (May to October) comparing the ERA40 driven model run with observation. (a) shows the mean summer temperature 1971-2000 in the reference dataset HYRAS, (b) the RMSE of the ERA40 driven model run compared to HYRAS and (c) the MSESS of the bias corrected run compared to the uncorrected.

where the temperature may exceed the range of temperatures in the historical period, which is only possible to a limited extent with classical quantile mapping (Maraun, 2016). However, the underlying assumption and the resulting constant transfer function might not be valid in a future climate (Pierce et al., 2015), leading to potential errors. Furthermore, the use of a parametric approach of fitting an assumed distribution to the data to derive the transfer function is still arbitrarily discussed.

160   Several studies, e.g. Pastén-Zapata et al. (2020); Qian and Chang (2021), apply a normal distribution for temperature to get a more robust transfer function. Using a fitted function has the additional advantage that the transfer function is independent of any smoothing interval that may be defined (Kerkhoff et al., 2014). On the other hand, parametric approaches introduce additional bias, if the distribution of a variable does not accurately match the theoretical distribution. Especially for extreme values, a deviating statistic is assumed according to the extreme value distribution. Quantile approaches, allowing different

165   statistical models for extremes, could potentially reduce uncertainty (e.g Vrac and Naveau, 2007; Berg et al., 2012; Schubert et al., 2017)

     As shown in Fig. 2, major improvements can be achieved by the distribution based QM using the example of T_{mean}. In panel (a) the reference data HYRAS is shown averaged over the summer half-year. Comparing this reference data to the simulations driven by ERA40, a root mean square error (RMSE) between $1.95\,^{\circ}\mathrm{C}$ and $2.18\,^{\circ}\mathrm{C}$ (5. to 95. percentile) is visible in the

170   evaluation area (Fig. 2b). The skill of the applied bias correction is expressed by the mean squared error skill score, MSESS, using the mean square error, MSE (Eq. (4)). MSESS is positive all over the domain (Fig. 2c), thus the correction leads to a better alignment of the simulation data with the observation. Stronger improvements coincide with regions of higher deviations of the uncorrected data.

$$\mathrm{MSESS} = 1 - \frac{\mathrm{MSE}_{\mathrm{corr,obs}}}{\mathrm{MSE}_{\mathrm{raw,obs}}} \tag{4}$$

2.3 Heat wave and impact indices

Different aspects of heat stress are addressed with this study. We start with the classical approach of describing the meteorological aspects of HWs. Secondly, we will focus on the impact on human health using a thermo-physiological description of heat. Finally, climate parameters – threshold-based indices that are tailored to the need of stakeholders in different fields of action – are evaluated. All metrics used are presented in the following.

2.3.1 Heat wave indices

A number of consecutive days with elevated temperature is called a HW. However, a universally fitting definition does not exist, but several definitions can be found in the literature. We here use the definition by Russo et al. (2014), in which a HW is defined as an uninterrupted series of at least three days where the daily maximum temperature $T_{\max}$ exceeds $T_{\max,90\%}$, the daily 90th percentile of $T_{\max}$ within a 31-day centered window over the reference period. Several metrics describing different aspects of HWs exist. The length of a HW is derived as the number of consecutive HW days, and its frequency is the average number of HW-days per year. As a measure for the HW temperature, we introduce the maximum excess temperature $\Delta T_{\max}$ above the 90th percentile threshold. Russo et al. (2014) proposed a Heat Wave Magnitude Index (HWMId), an index that can be compared across regions and time, taking HW length as well as temperature into account. The HWMId is calculated as

$$\text{HWMId} = \frac{T_{\max} - T_{\max,25\%}}{T_{\max,75\%} - T_{\max,25\%}} \tag{5}$$

with $T_{\max,25\%}$ and $T_{\max,75\%}$ the daily 25th and 75th percentile of $T_{\max}$ within a 31-day centered window in the reference period. The event sum over the heat event characterizes the magnitude of a HW.

2.3.2 Human heat stress

Apart from air temperature, there are additional elements such as clothing, humidity, mean radiant temperature, air movement, and metabolic rate that determine a person's level of thermal comfort (Fanger, 1970). With the requirement to transform this complex system into an application-friendly model, the universal thermal climate index (UTCI) was developed in 2009 from an interdisciplinary collaboration between human thermophysiology, physiological modeling, meteorology and climatology (Jendritzky et al., 2008). The index is defined as the air temperature of a reference condition causing the same thermal comfort as the actual response. The reference conditions were determined as a wind speed $\text{WS} = 0.5\,\text{m s}^{-1}$ at 10 m height and a mean radiant temperature T_{mrt} equal to air temperature T_{air}. The relative humidity in the reference environment is 50 % for temperatures below 29 °C. However, for temperatures above 29°C, the water vapour pressure is instead kept constant at a level of 20 hPa (Błażejczyk et al., 2013). In Table 3, the defined categories for heat stress are listed. The calculation of the UTCI is based on Fiala's multi-segment model of human physiology and thermal comfort (Fiala et al., 2012), coupled with a clothing model by Havenith et al. (2012). Details can be found in e.g. Jendritzky et al. (2012); Fiala et al. (2012); Havenith et al. (2012). The hourly model results were taken as input for the calculation of UTCI in this study. Due to missing hourly, gridded observations, no bias correction was applied.

Table 3. Assessment scale of heat stress using the UTCI. Cold stress for UTCI $\leq 9\,^{\circ}$C is not shown here.

UTCI in $^{\circ}$C	Category
9 to 26	no thermal stress
26 to 32	moderate heat stress
32 to 38	strong heat stress
38 to 46	very strong heat stress
above 46	extreme heat stress

2.3.3 User-tailored Climate Indices

More and more sophisticated indices were developed, focusing on different aspects of heat stress. However, in order to take action in the local governments, the exact information on the change of climatic conditions is not always helpful – on te contrary. The so-called "climate information usability gap" is the barrier about what scientists see as useful and what users consider useful for their decision-making. One key aspect of narrowing the gap is the customization and tailoring of the data to the user's need to improve the usability of climate information (Lemos et al., 2012), often as a co-design approach. In the case of climate adaption strategies, the measures of interest are according to Hackenbruch et al. (2017) meteorological events leading to an effect on people/health risks (for example, hot days), influence on capital investments or municipal budgets (for example, winter services) or property damage (for example, heavy precipitation events).

To assess the impact of changing temperature, we present several user-tailored climate parameters following Hackenbruch et al. (2017). The selected parameters, their definition, and field of action are summed up in Table 4. All parameters are related to regional temperature changes but cover different fields of action and therefore are of concerns of different stakeholders. The aim of the choice is to show the diversity of the effects of climate change and to present the potential of high-resolution climate models for climate adaptation.

3 The added value of temperature in a convection permitting ensemble

An evaluation of the uncorrected raw output of the ERA40 driven CCLM simulations compared to the observations shows a cold bias in the simulations over Germany. Figure 3a shows that in the reanalysis-driven simulation, the median monthly temperature over the evaluation domain in the 7 km simulation (blue thick solid line) is always lower than in the observation (gray thick solid line). This deviation is larger in the summer months. A similar pattern is found for further percentiles of the distribution, as shown for example for the 10th and 90th percentiles (thin lines in Fig. 3a), as they are generally underestimated, especially in summer. However, the 7 km output occasionally exceeds the observation in single autumn and winter months (October for the 90th and January for the 10th percentile). In the convection permitting simulation (2.8 km), the monthly median temperature in the warm season is comparably higher than in the coarser simulation, leading to a reduced cold bias. In autumn it even exceeds the observation by 0.6 K. However, there is no strong improvement in the mean temperature during the

Table 4. Definition and field of action of the tailored climate parameters related to temperature development based on the KLIMOPASS project (Schipper et al., 2016). T is daily mean, max or min temperature, T_{JJA} and P_{JJA} are the mean daily temperature and precipitation sum from June to August. The subscript *clim* refers to the climatological mean, that was calculated over the reference period 1971-2000. The lower limits of T_{max} for walking weather are: $0\,°\mathrm{C}$ for Dez, Jan, Feb, $5\,°\mathrm{C}$ for Mar and Nov, $10\,°\mathrm{C}$ for Apr, May, Sep, and Oct, and $15\,°\mathrm{C}$ for Jun, Jul, and Aug.

Climate Index	Definition	Field of action
Very hot days	$T_{\mathrm{max}} > 35\,°\mathrm{C}$	Road construction: Damage to roads and so-called „blow ups" occur due to strong heating of the road concrete. Health: Decrease in mental and physical performance.
Tropical nights	$T_{\mathrm{min}} > 20\,°\mathrm{C}$	Health: impaired regeneration
Growing days	$T_{\mathrm{mean}} > 5\,°\mathrm{C}$	Conservation: Critical to ecosystem composition and development. Forestry: Determines the window of opportunity for forest work. Agriculture: Impacts the growing zones for certain crops
Dry hot summers and years in between	$T_{\mathrm{JJA}} > T_{\mathrm{JJA,clim}} + 1\,°\mathrm{C}$ & $P_{\mathrm{JJA}} < 0.8 \times P_{\mathrm{JJA,clim}}$	Agriculture, Forestry: Reduced primary productivity of forest and grassland as well as tree mortality at higher extremes. Urban planning: Adaption of tree species and assessment of necessary irrigation. The interval in between hot dry summers is essential for recovery. E.g. 5 years are estimated for tree recovery.
Conditions for drosophila suzukii	$T_{\mathrm{mean}} > 10\,°\mathrm{C}$ & $T_{\mathrm{max}} < 30\,°\mathrm{C}$	Agriculture: Changing climate can influence pests. For each crop and pest, conditions have to be assessed separately. The drosophila suzukii, which is a major pest for fruit production in Central Europe is taken as one exemplary quantity.
Walking weather	$T_{\mathrm{max}} < 25\,°\mathrm{C}$ & $T_{\mathrm{max}} >$ variable lower threshold (see table description)	Tourism

230 winter months, and the cold bias persists. A consistent reduction of the cold bias is found for the 10th and 90th percentiles, but possible overestimation of higher percentiles seems to become more frequent, especially in late summer and autumn. In the convection permitting ensemble, monthly mean temperature is improved similarly as shown in dashed lines in Fig. 3a. Again, the largest improvement is in the summer. However, the mean bias in the ensemble median is larger than in the reanalysis, especially in the winter.

235 Averaged over all grid points, the mean error in the reanalysis-driven simulations is reduced from $-1.1\,°\mathrm{C}$ to $-0.13\,°\mathrm{C}$ in the summer half-year (Fig. 3b). Moreover, the spread is increased. In the winter half-year the median is reduced from $-0.69\,°\mathrm{C}$ for 7 km to $-0.56\,°\mathrm{C}$ for 2.8 km. This is a smaller but still significant reduction confirmed by a Wilcoxon signed-rank test. The test was applied to the two fields of mean error of the coarser (7 km) and convection permitting (2.8 km) simulations. The null hypothesis of zero difference between the errors was rejected by the test based on a significance level of 0.05. Those patterns
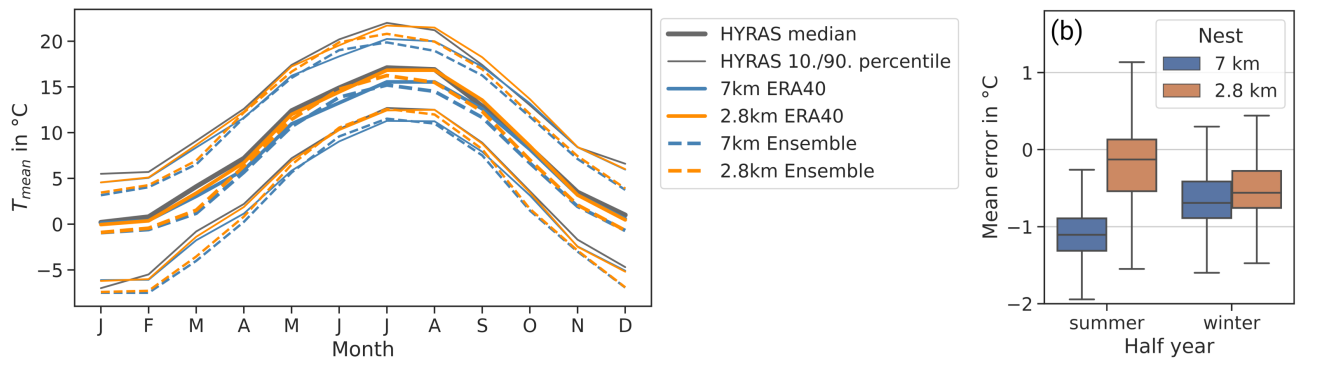
Figure 3. Raw output of 2 m temperature in the 2nd (7 km) and 3rd grid (2.8 km) in comparison with the observation dataset HYRAS for the reference period. The analysis was performed on the grid points in the evaluation area. (a) shows the monthly mean temperature in the observation (black solid lines) compared to the reanalysis results (colored solid lines) and the median of the ensemble members (dashed lines). The thick line represents the median in the reference period and in the evaluation area, the thin lines show the 10th and 90th percentiles respectively. (b) visualizes the mean error of ERA40 time series compared to the observation for summer (May–Oct) and winter half-year (Nov–Apr). The boxplot shows the spread over the grid points.

240   in the temperature output from coarse to high resolution are similar in the ensemble as in the reanalysis-driven run. For further information on the performance of the single ensemble members, please refer to the supplementary information (Fig. S1).

To reveal spatial patterns, the mean summer half-year temperature of the 2nd, 7 km nest (Fig. 4a) and the 3rd, 2.8 km nest (Fig. 4b) of the reanalysis-driven run are compared to the observation (Fig. 2a). Whereas there is a negative bias at nearly all grid points for the coarser nest (Fig. 4a), local differences are visible for the convection permitting simulation (Fig. 4b). Here, a

245   negative bias is still present in the north of the domain, especially in the hilly regions. In the south of Germany, predominantly positive anomalies are visible. Even though the regions with positive bias are not correlated with altitude, they do not seem to be independent of orography. The largest positive bias is found in the South German Scarplands (lon $\approx 9.0\,°$, lat $\approx 48.5\,°$) – located directly between two major mountain ridges, the Black Forest and the Swabian Alps.

For nearly all grid points, there is an improvement with the convection permitting simulation, which is indicated by a positive

250   MSESS in Fig. 4c comparing the second and third nest with respect to the reference dataset HYRAS. There are a few grid points with negative MSESS. Those are associated with a positive bias and an overshoot of the convection permitting simulation.

The density distribution of daily summer temperature shows nearly perfect agreement of observation and the convection permitting reanalysis run (Fig. 4d). In comparison, the distribution for the reanalysis-driven 7 km simulations is shifted towards colder temperatures and has a lower spread. Especially the highest summer temperatures are better resolved by convection

255   permitting simulations. An improvement is also visible for the 2.8 km median of the ensemble simulations compared to the 7 km output. However, especially the high summer temperatures are still underestimated by the CPM. Low temperatures, from approximately $-3\,°C$ to $10\,°C$, are overestimated.
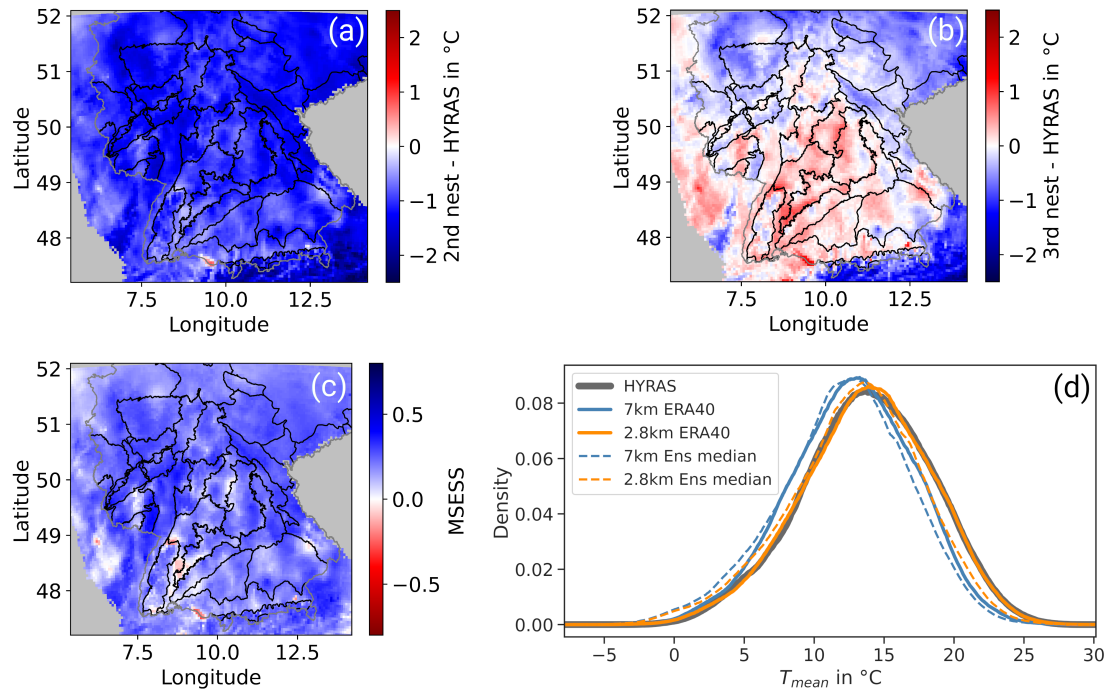
Figure 4. Evaluation of ERA40 driven simulation on a convection parametrizing (7 km) and convection permitting (2.8 km) scale for the summer half-year (May–Oct) in the period 1971-2000 compared to the reference observation datas et HYRAS. The difference of the raw output of mean summer temperature is shown (a) for the 7 km simulation and (b) for the 2.8 km simulation. In (c) the MSESS of 2.8 km compared to 7 km is mapped and (d) displays the density distribution of 2.8 km and 7 km in the evaluation area for the reanalysis driven run (solid lines) and the median of the ensemble in the reference period (dashed lines).

Overall, we identify a significant reduction of the mean bias for the convection permitting resolution, which is especially pronounced during summer. Over Germany, the convection permitting simulation reproduces a realistic frequency distribution of daily 2 m temperature. The remaining mean errors show a trend from negative bias in the north toward positive bias in the south. Other local patterns are partly associated with the predominant landscape regions. Based on the added value found in the 2.8 km resolution, its output is used for the following analysis.

4   Regional temperature trends

Annual cycle Future temperature is not expected to develop evenly over the year. In the study area, the smallest increase is observed in spring, largest in late summer and during winter (Fig. 5a). The behavior is similar for GWL2 and GWL3. The stronger late summer increase leads to a shift of the summer peak of maximum temperature by 12 days in GWL3 compared to 1971-2000.

A closer view in the ensemble spread shows that throughout the year, there seems to be good agreement within the three simulations driven by EC-EARTH, MPI-ESM-LR and CNRM-CM5. There is an ensemble variance of $0.6 \, \mathrm{K}^2$ for the mean temperature averaged over the study area in GWL3. In contrast, warming – especially in the winter and autumn – is significantly more pronounced in the simulation driven with HadGEM2-ES (Fig. 5a, dotted line). Averaged over the year, the temperature increase is 1.5 K higher than for the other simulations by GWL3. HadGEM2-ES is the member with the highest climate sensitivity of the driving GCM within this ensemble (cf. Nijsse et al. (2020); Table 1). In the following, the presented results of HadGEM2-ES will stand out repeatedly as it appears that the nature of its projected climate change signal differs from that in the other three ensemble members EC-EARTH, MPI-ESM-LR, and CNRM-CM5 with lower climate sensitivity.

Temperature distribution Figure 5b shows the density of the daily mean summer temperatures over the evaluation area. The peak of the distribution in the evaluation period is at 14.2 °C. The shape of the distribution is reproduced well compared to the observation, however, the ensemble overestimates the probability at the peak of the distribution. In a warmer world, the mode shifts to higher temperatures that are 15.4 °C in GWL2 and 16.6 °C in GWL3. Moreover, higher maximum temperatures up to 27.4 °C (99th percentile) in GWL3 are reached. There is a decline in temperatures left of the peak, respectively. However, especially for low temperatures, the magnitude of decrease is relatively small, leading to an increased width of the distribution. A parametrization of the spread of the distribution is made in terms of the Full Width of Half Maximum (FWHM), which is defined as the width of the distribution at the level of the half peak value. As shown in Fig. 5c the FWHM in the ensemble average increases from 10.4 to 12.1 °C. Three out of four ensemble members agree on a steady increase of the width. Only the simulation run by HadGEM2-ES does not confirm an increase of FWHM in the period from 1971-2000 to GWL2. Regarding the temperature distribution, an increasing FWHM indicates a more variable daily temperature, leading to higher amplitudes and to a stronger increase in the frequency of warm extremes on the right side of the curve compared to the shift of the curve median.

Spatial patterns The average summer temperature (May–Oct) varies significantly over the evaluation area as already shown for the observational data in Fig. 2a and provided in the supplementary information (Fig. S2) for the ensemble mean. It ranges from 12.3 to 15.5 °C (5. and 95. percentile). As expected, the highest temperatures are found at low altitudes. The Rhine Valley stands out with the highest average temperatures up to 16.6 °C. The lowest average temperatures are accordingly observed in complex regions with pronounced orography: Examples are the Harz (average 12.5 °C) in the Central Uplands or the Black Forest (average 13.0 °C) in the south. Moreover, spatial heterogeneity is increased in those complex regions.

The summer temperature increases with global warming over the whole evaluation area. From the reference period (global warming at 0.46 °C) to GWL2, the increase is on average 1.55 °C (Fig. 6a). From the reference period to GWL3, the average increase is 2.60 °C (Fig. 6c). When integrated over the year, the ensemble shows a slightly stronger warming than only over the summer months, indicating that summer temperatures are less sensitive than the annual mean (Fig. 5a). However, the differences are still in the range of 0.11 °C (0.09 °C) above the global warming in GWL2 (GWL3). Therefore, the regional warming in the evaluation area in the considered GCM-RCM combinations is close to the global average and only slightly enhanced. This is less than suggested by the theory of greater warming over land than over the ocean and as generally projected (IPCC, 2021).
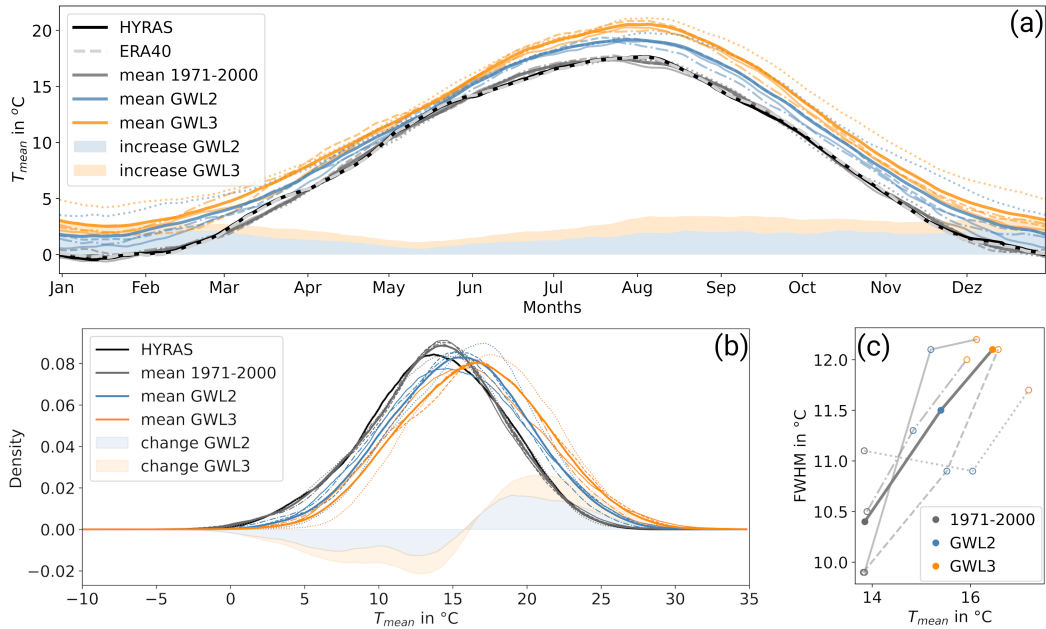
Figure 5. The different aspects of the evolution of daily mean temperature T_{mean} from reference period (gray) over GWL2 (blue) to GWL3 (orange) are shown. (a) displays its annual cycle averaged over the study area and over a 31-day running window. (b) shows the density distribution of daily mean temperature in the summer half-year (May–Oct) and (c) its full width at half maximum (FWHM). Different line styles correspond to different driving GCMs – solid: MPI-ESM-LR, dashed: EC-EARTH, dash-dotted: CNRM-CM5, dotted: HadGEM2-ES, the thick lines correspond to the ensemble mean.

The impact of the bias correction is considered to be negligible, as the uncorrected data integrated over the year show a nearly identical warming of $0.11\,°\mathrm{C}$ ($0.07\,°\mathrm{C}$) above the global average in GWL2 (GWL3) in the evaluation area.

Geographical dependence leads to regional variations of warming. Over the evaluation area, warming ranges from 1.45 to 305 $1.64\,°\mathrm{C}$ (5th And 95th percentiles) in GWL2 and from 2.44 to $2.76\,°\mathrm{C}$ in GWL3. As shown in Fig. 6a and 6c, the strongest increase is observed in the uplands in the north of the domain (GWL2), and in the Black Forest and Swabian Alps in the south (GWL2 and GWL3). Less warming, below the global average, is expected in the Alpine Foreland (GWL2 and GWL3).

The ensemble spread increases from GWL2 with 1.06 to $1.47\,°\mathrm{C}$ to GWL3 with 1.12 to $1.48\,°\mathrm{C}$ (5. and 95. percentile). Data show a trend superimposed from north to south with decreasing spread (Fig. 6b and d) Moreover, the ensemble spread seems to 310 depend partially on the orography and landscape. It is especially high in the north west of the domain and in areas with higher elevation. Lowest spread is visible in the flat Rhine Valley. The higher deviations at the locations of the large lakes in Southern Germany (Lake Constance (lon 9.4; lat 47.6), Lake Ammersee (lon 11.1; lat 48.0), Lake Starnberg (lon 11.3; lat 47.9), Lake Chiemsee (lon 12.5; lat 47.9)) are caused by interpolation of the water surface temperatures from the coarse grid, since no lake module was applied.
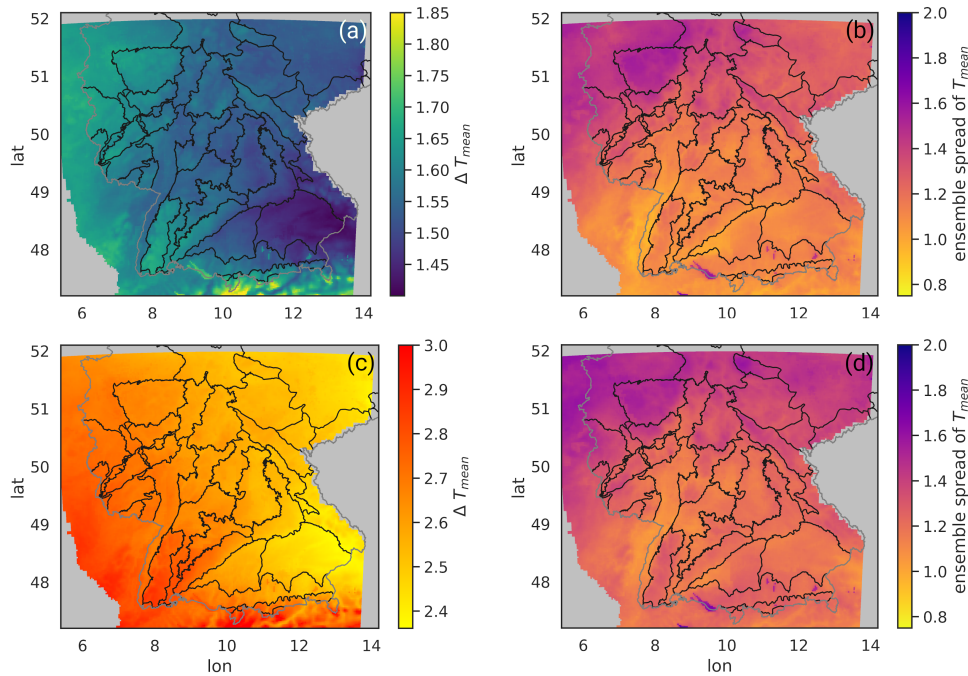
Figure 6. Mean development of T_{mean} in the summer half-year (May–Oct) as ensemble mean compared to the reference period for GWL2 (a) and GWL3 (c) and the according ensemble spread calculated as range between minimum and maximum prediction for each grid point in GWL2 (b) and GWL3 (d).

Summing up, the mean temperature over Germany rises in a warmer climate predominantly in late summer as well as in the winter half-year, with the smallest increase in spring. This leads to a general shift of the summer maximum temperatures to later summer. The increase is spatially largely homogeneous, with slightly stronger warming expected in mountainous regions. Moreover, the temperature distribution in a warmer climate is expected to be wider (larger variability), indicating that extreme temperatures will experience a greater change compared to the average warming.

5 Heat wave characterization

This section characterizes HWs in the future based on their different features – length, temperature, magnitude, and frequency. Be aware that throughout this section we are focusing on a relative definition of these events – an anomaly versus the 90th percentile from the reference period (Sec. 2.3.1). The relationship between HW magnitude, duration, and excess temperature is examined for the most severe HWs in each year in terms of the cumulative HW magnitude in the evaluation area (Fig. 7). The according figure providing absolute HW temperatures is provided in the supplementary (Fig. S3).
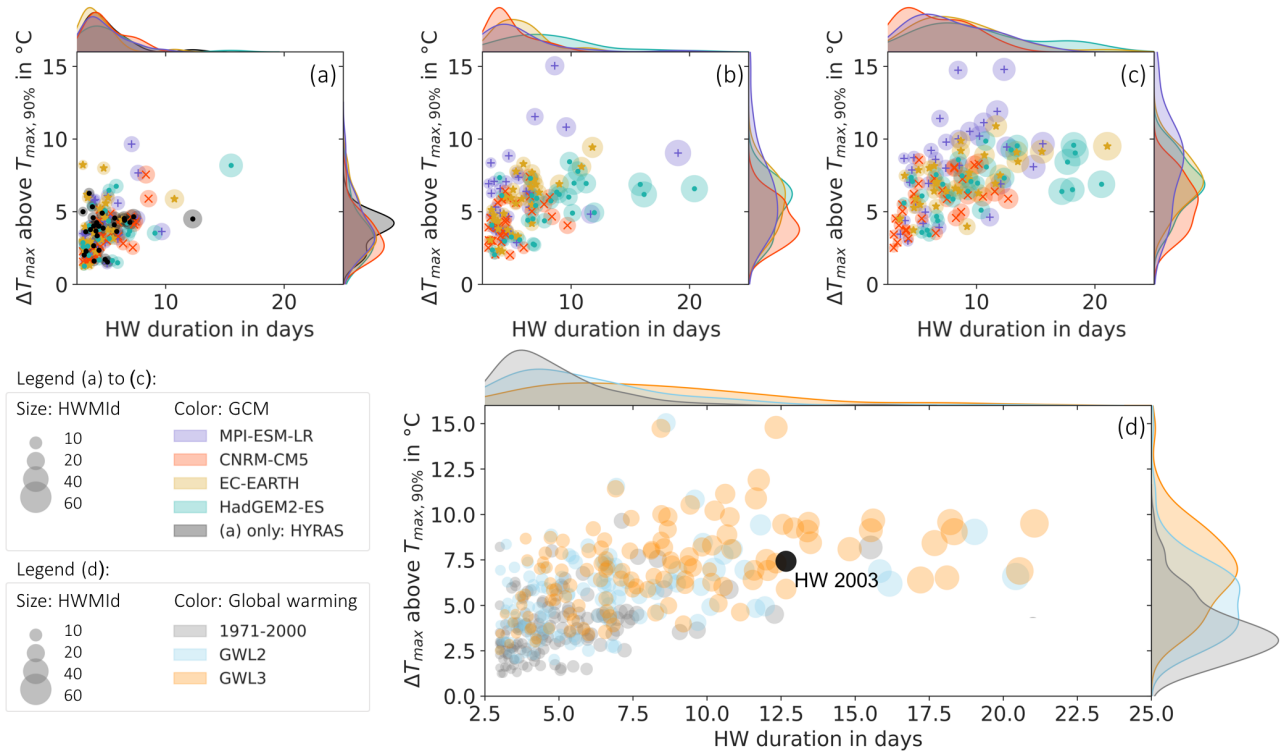
Figure 7. The bubble plots show the strongest HW in each summer half-year (May-Oct) in every projection run with respect to duration on the abscissa and excess temperature on the ordinate. Bubble size indicates mean HWMId over all grid point results affected by the HW. Marginal plots show the distribution of duration of the heat waves in days (abscissa) and the distribution of the excess temperature (ordinate). Panel a to c show the single ensemble members and comparison with the observation: a for 1971-2000, b for GWL2, and c for GWL3. Panel d shows the total set of all of the heat waves from the single ensemble members for 1971-2000, GWL2 and GWL3. The black data point corresponds to the HW in 2003 derived from HYRAS data.

Firstly, the observed HW characteristics in the reference period (1971-2000) are analyzed, as shown in black in Fig. 7a. The average duration of the strongest HWs per year ranges from 3 to 12 days. The temperature excess $\Delta T_{\max}$ above the 90th percentile ranges from 1.5 to 6.3 °C. The longest observed HW reaches up to 12 days, however, the correlation with excess temperature is weak ($r = 0.22$). The observed HWMId has a range of 5 to 22, with an average of 8.8. HWMId increases with 330 HW length ($r = 0.99$).

To evaluate the representation of the three HW characteristics in the ensemble projection, the results of observation and simulations in the reference period are compared (Fig. 7a). The HW duration is reproduced well by all ensemble members and no significant deviation from the observed distribution of duration (marginal distribution on the abscissa) is visible, which is confirmed by a two-sample Kolmogorov-Smirnov test on the level of significance of 0.05. Also for the HWMId, the test 335 confirms no significant deviation between simulation and observation. For the excess temperature, no significant deviation

from the observed distribution is found for three out of four ensemble members. However, significant differences for the results of the CNRM-CM5-driven simulation and an underestimation of the simulated excess temperature is visible in the marginal distribution on the ordinate (Fig.7a). Moreover, there is a peak around $\Delta T_{\max} = 4\,°C$ in the observation that is not reproduced by any ensemble member. The ensemble of climate simulations shows no significant deviation from the observed distributions in the reference period for the characteristics duration and HWMId, confirmed by a two-sample Kolmogorov-Smirnov test on a level of significance of 0.05. For the excess temperature, the test results support no significant deviation from the observed distribution for three out of four ensemble members but significant differences for the results of the CNRM-CM5-driven simulation. The underestimation of the modelled excess temperature is shown in Fig.7a. Moreover, a peak around $\Delta T_{\max} = 4\,°C$ is visible in the observation that is not reproduced by any ensemble member.

The climate change signal of excess temperature (1), duration (2), and magnitude (3) develops differently in the four ensemble members (Fig. 7b and c), but superimposing the three GWLs, a clear picture of HW intensification emerges (Fig. 7d). (1) All ensemble members agree on an increase of average excess temperature and an increased width of its distribution compared to the reference period. The highest excess temperatures are found for MPI-ESM-LR-driven simulation up to $\Delta T_{\max} = 15\,°C$ in GWL2 and GWL3. The lowest excess temperatures are projected by the simulation driven by CNRM-CM5, that already showed an underestimation in the reference period. In the ensemble median, there is a shift towards higher HW excess temperatures up to 5.3 (GWL2) and 6.9 °C (GWL3) (Fig. 7d). This implies that with HW excess temperatures from 2.6 °C to 4.5 °C (25 and 75 % confidence interval) in the reference period hardly any HW are occurring today, that will be a common scenario in the future. (2) Also for HW duration, a future increase in mean and spread of the distribution is detected by all ensemble members. Again, the smallest changes are projected by the simulation driven by CNRM-CM5. The simulation driven by HadGEM2-ES projects in general the longest HWs. These discrepancies in HW duration indicate different dynamics in the driving models. In fact, HadGEM2-ES is described as one of the best performing CMIP5 GCMs in past climate for weather types (Perez et al., 2014) and blocking, which is underestimated in CMIP5 models in general (Brands, 2022). Presented extremely long HWs should therefore not be discounted as an outlier, but treated with caution. In the ensemble average, there is a clear shift towards longer HWs. The average duration increases from 4.3 (reference) over 5.1 (GWL2) to 7.5 days (GWL3). Moreover, the spread increases drastically which leads to maximum HW duration up to 21 days. (3) The development of HWMId is strongly correlated with HW duration in the simulations. In the ensemble, a 26 % (100 %) increase in the median of HWMId is expected from reference to GWL2 (GWL3) (HWMId in reference: 8.2, GWL2: 10.3, and GWL3: 16.5). The significance of the increase of duration, excess temperature and HWMId are confirmed by a two-sample Kolmogorov-Smirnov test on the level of significance of 0.05.

In order to put the results into perspective, they are compared with an actual reference event for Germany – the HW in 2003. A HW with a strong economic and environmental impact and cause of thousand deaths, referred to as a record HW (e.g., De Bono et al., 2004). Performing an analog analysis on 2003 HYRAS data, this HW had an average length of 12.7 days, maximum excess temperature of 7.4 °C and HWMId of 26.7. It is visualized in black in Fig. 7d. As expected the event is extremely unlikely in the reference period. Only one simulated summer in the reference period by HadGEM2-ES exceeds the measured event in 2003. In a warmer world, events with such a strength occur with higher probability. In GWL3 such an event
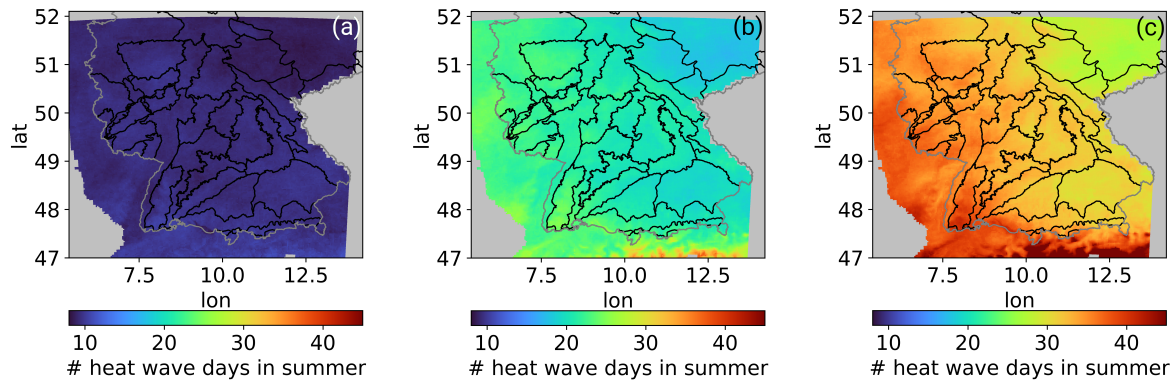
Figure 8. The ensemble mean of average number of HW days per summer half-year (May–Oct) in 1971-2000 (a), GWL2 (b), and GWL3 (c).

is in the 25 % confidence interval of 5.3 °C to 8.4 °C . For duration, the HW 2003 exceeds the 25 % confidence interval of 5.1 to 10.4 days in GWL3 and its duration is ranked 16th in the projections of 4×30 years, corresponding to an 8-year return period in GWL3. For HWMId, its rank of 21 in GWL3 leads to a 6-year period. It should be noted that in this case no distinction is made between ensemble members. The variations between ensemble members discussed earlier indicate the range of uncertainty in
375 this projection. Moreover, the analysis considers only the local observations of 2003 limited to the simulation area. Summing up, an event like HW 2003 will become more likely but is projected to stay an extreme event with a return period of 5 to 10 years.

To assess regional patterns, the cumulative number of HW days as measure of HW frequency is analyzed (Fig. 8). Again the summer half-year is considered only. In the reference period, averaged over 30 years, few HW days are observed per summer
380 half-year. In the evaluation area, the number of HW days ranges from 8.7 to 9.9 (5th to 95th percentile) and is distributed relatively uniformly across space. An overall increase from 18.8 to 23.0 (5th to 95th percentile) HW days is simulated in GWL2. With even more warming in GWL3, spatial features become visible. The increase affects predominantly the southwest. Moreover, slightly enhanced HW occurrence is projected in regions with higher elevation as the Black Forest. Over the domain, 28.7 to 36.9 (5th to 95th percentile) HW days are expected in GWL3.
385 The analysis of the seasonal changes reveals that HW severity is distributed inhomogeneously over the summer (Fig. 9). In the reference period the occurrence of large HWs, defined as HW with a coverage of at least 50 % of the study area, is relatively flat distributed. There is a declining trend of the probability throughout the summer. From GWL2 to GWL3, it is apparent that there is an increased HW occurrence in late summer, around August and September. All members of the ensemble agree on this trend. However, the magnitude and timing of the adjustment varies. The highest HW probabilities are projected by EC-EARTH
390 and HadGEM2-ES. Some ensemble members even depict a decrease in the occurrence of large HW in early summer in GWL2 (May to June).
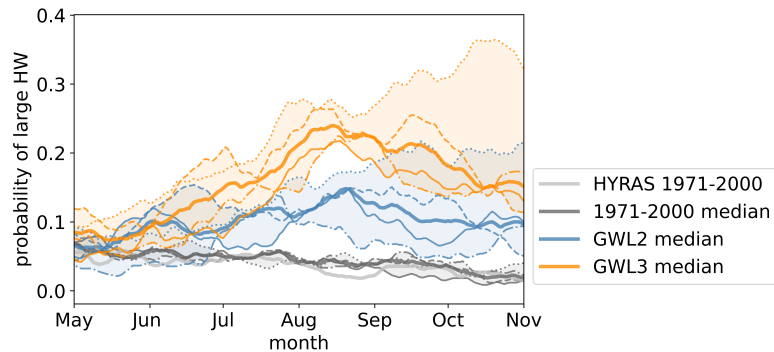
Figure 9. Probability of large HW (coverage $\geq 50\,\%$ of the evaluation area) over the summer (May–Oct) calculated over a 31-day running window. The thick line corresponds to the ensemble median, whereas the different line styles of the thin lines correspond to different driving GCMs – solid: MPI-ESM-LR, dashed: EC-EARTH, dash-dotted: CNRM-CM5, dotted: HadGEM2-ES.

Analysis of both regional and seasonal patterns supports that HW frequency is closely linked to the future temperature increase, for which a similar spatial pattern and annual cycle of the change signal was found. However, it should be noted, that while the average temperature increases by only 2.6 °C from the reference period to GWL3 (Sec. 4), this translates into an enormous increases of HW frequency of more than factor three. This amplified increase of HW frequency is attributed mainly to a higher change of higher percentiles compared to the increase in mean temperature (Sec. 4). Furthermore, more persistent weather patterns potentially enhance the severity of HWs in a future climate (Kyselỳ, 2008).

In summary, future HWs are characterised by significantly higher temperatures and longer HW duration. Thus, the magnitude of HWs increases dramatically in a warmer future, namely by 26 % (100 %) in GWL2 (GWL3). Furthermore, enhanced variability is projected for the HW characteristics. While the increase of HW days is spatially largely homogeneous, there is clear seasonality, with a strong increase in HW occurrence in late summer.

6 Impacts of temperature and heat increase

The meteorological perspective leaves open the question of the impacts of heat extremes, which will be addressed in the following section. The focus is first on human heat stress, then the analysis is extended to further heat-related climate parameters.

Human heat stress The number of days with UTCI > 32 °C are defined as days with strong human heat stress. As outlined in methods, UTCI is derived from hourly data. Due to missing gridded hourly observations, it was not subjected to bias correction. As a consequence, there is a larger ensemble spread in the UTCI. There is good agreement between three of the four ensemble members, showing a similar range of UTCI over the reference period 1971-2000. The simulation driven by HadGEM2-ES results in a significantly higher number of days with UTCI > 32 °C. We attribute this difference mainly to higher summer temperatures in this simulation, which unlike the previous analysis of daily data, was not subject to bias
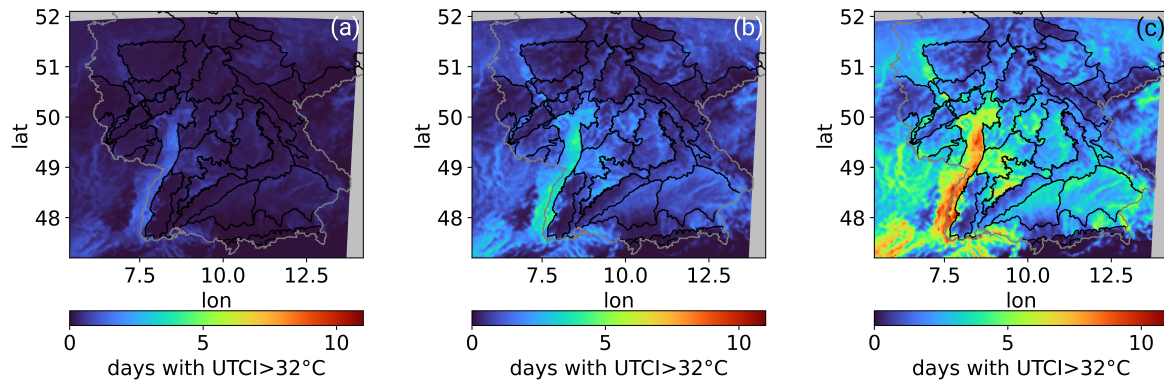
Figure 10. Ensemble median of number of days per year with strong human heat stress defined by UTCI $> 32\,^{\circ}$C for 1971-2000 (a), GWL2 (b), and GWL3 (c).

correction. To minimize the influence of possible outliers, we consider the ensemble median in the following analysis. The spatial distribution is displayed in Fig. 10. In the reference period hardly any days per year with strong heat stress are found. The range over the evaluation period is 0.0 to 0.6 days per year (5 to 95 % confidence interval). A maximum number of up to 2.0 days per year averaged over the reference period in flat regions is visible in the ensemble.

415   The average number of days with strong heat stress rises in the future GWL2 all over the domain – on average by 0.6 days per year – but with notable spatial differences. Again highest numbers of heat stress days are in the flat Rhine Valley with up to 5.1 days per year (Fig. 11a). Moreover, this region shows the strongest increase from reference to GWL2 which is on average 1.8 days per year. For GWL3, this pattern intensifies with a non-linear, rather exponential increase with global warming (Fig. 11a). Up to 10.7 days per year with strong heat stress are projected in the hottest region. Also in regions with higher elevation, there

420 is a significant increase of future heat exposure, on average 2.3 days are for example expected in the Black Forest by GWL3. For comparison, this exceeds the heat stress that prevailed in the mild, flat Rhine Valley during the reference period.

    User-tailored climate parameters The analysis of the six tailored climate parameters shows how changing temperature affects further fields of action (Fig. 11b-g). To visualize regional effects, results of two German landscape regions are added to the graph in addition to the entire evaluation area: the flat and warmest region of the model domain, the Rhine Valley (dotted

425 boxes) and as counterpart, striped boxes show the Black Forest region, which is geographically directly adjacent to the Rhine Valley and, as a low mountain range, has a high altitude and complex orography (cf. Fig. 1).

    Most drastic changes of the mean values are projected for very hot days, tropical nights and dry hot summers (Fig. 11b, c, d). In addition, for very hot days and tropical nights a non-linear, rather exponential increase with global warming is projected. This coincides with a significant increase of variance. The behavior of very hot days and tropical nights is comparable to

430 UTCI (Fig. 11a), implying that this amplified, non-linear increase might be preferentially associated with strong heat stress. The pattern is observed for all shown landscape regions. Differences appear in the absolute values: Heat stress is especially
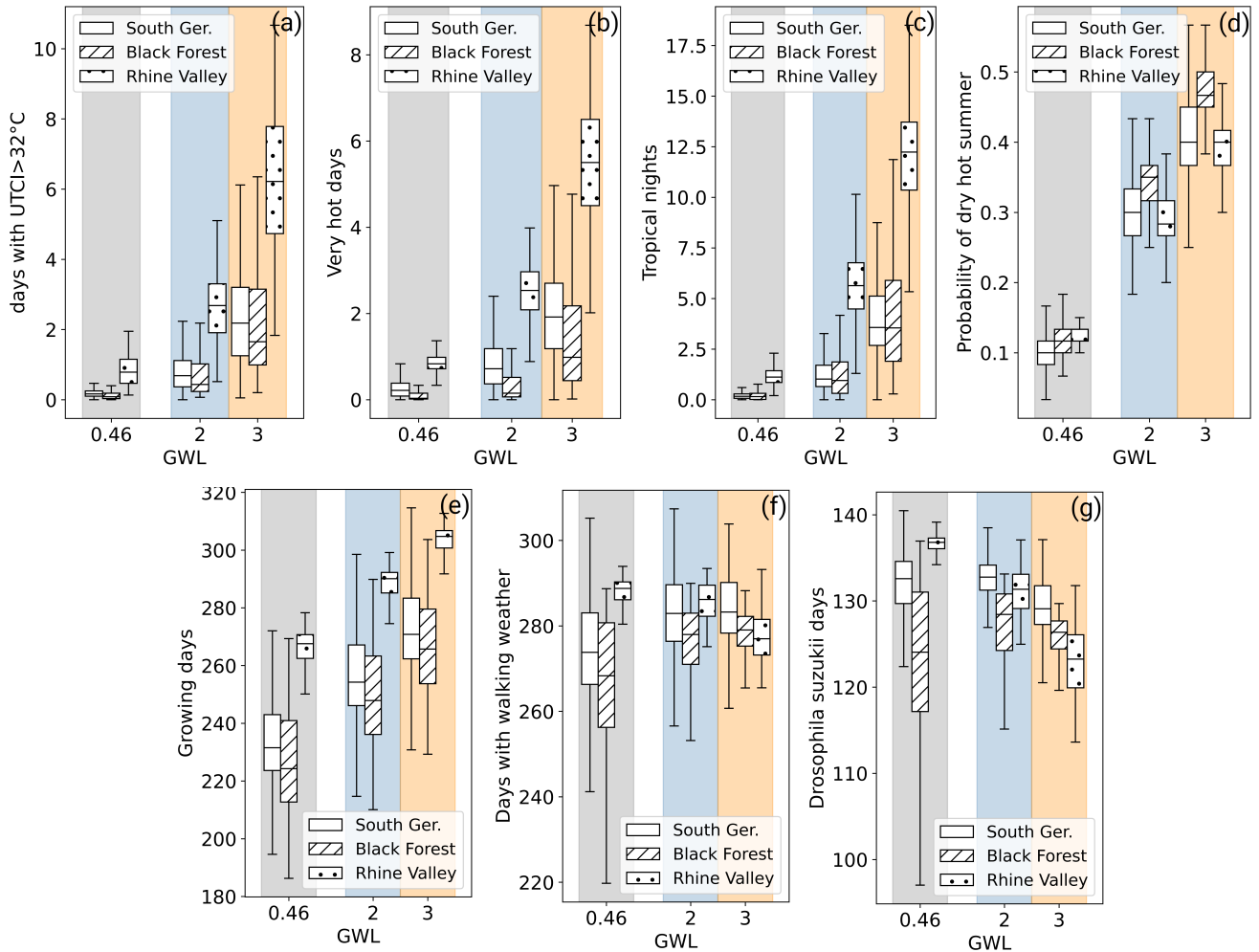
Figure 11. Ensemble median of UTCI and climate parameters over global warming. The global warming level of the reference period is assumed to be 0.46 K based on Teichmann et al. (2018). The empty box plot visualizes the distribution over the evaluation area, striped boxes represent results in the Black Forest, and dotted in the Rhine valley.

pronounced in the Rhine Valley at low altitude where it exceeds the values in the adjacent Black Forest by a factor of 3.7 (very hot days) or 2.8 (tropical nights) in GWL3.

An about mean linear increase with global warming is visible for dry hot summers and growing days (Fig. 11d and e). Growing days are expected to increase on average by 39 (evaluation area), 40 (Black Forest), 37 (Rhine Valley) days from reference to GWL3, indicating that dependency of the change signal on the region is negligible. Existing regional patterns and variability within a landscape region appear to be preserved in a warmer climate and mean values are subjected to a shift only.

The probability of dry hot summers increases approximately linear as well, accompanied by increasing spatial variance. Here, largest increase is observed in the Black Forest, the smallest in the Rhine Valley. Overall, the probability of a dry hot summer increases drastically: From the reference to GWL3, the projected mean increase corresponds to a factor of 4 (Evaluation area and Black Forest) or 3.2 (Rhine Valley).

The two remaining parameters are examples designed for specialized applications in individual, often region-specific challenges – here walking weather for tourism strategy (Fig. 11f) or pests e.g. drosophila suzukii for agricultural planning (Fig. 11g). Using days with walking weather as an example, their number increases in the Black Forest and the variability decreases. The trend in the Rhine Valley is opposite, a decreasing number of days with walking weather with increasing variance. Hence in GWL3, relatively similar numbers of days are to be expected in the two contrasting regions. Also for days with conditions for drosophila suzukii, no common trend can be identified and the examples show a climate change signal that depends crucially on local conditions. Such behaviour is mainly attributed to the more complex definition of the parameters with an upper and a lower limit. The evaluations indicate that the more complex the parameter – or the underlying challenge in climate adaptation – the more important the regional consideration becomes.

We conclude that the changes regarding UTCI and user-tailored climate parameters do not necessarily scale linearly with global warming. An over-proportional increase of the climate parameter with global warming is preferably the case for parameters that describe strong heat stress. Moreover, the change signal of climate parameters depends crucially on the landscape region. In particular for parameters describing strong heat stress, the absolute change signal is highest in flat regions that are already exposed to the greatest heat today. For specialized applications, parametrized over more complex climate parameters, region-specific trends are expected.

7 Discussion and conclusion

In the presented analysis of heat extremes and related impacts in a convection permitting climate ensemble for Germany, we could draw three main conclusions:

1. We found an added value for simulated temperature in the convection permitting ensemble, especially for hot temperatures, that goes beyond better representation of the topography only. The improvement is particularly prominent in the summer half-year.

2. Mean temperature in the warm season in Germany increases largely homogeneous in space. An increase in temperature variability is found in future projections, which favors the development of longer and hotter HWs, especially in late summer. Heat wave magnitude is expected to increase by 26 % (100 %) in GWL2 (GWL3).

3. The changes in human heat stress (UTCI) and tailored climate parameters show a clear dependence on the major landscapes. Heat stress is particularly prominent for low land areas like the Rhine Valley. An over-proportional increase of parameters associated with strong heat stress is found. For the change signal of more complex tailored climate parameters, linear behaviour and/or strong dependency on the landscape can be identified.

470   Our results show an improved representation of the 2 m-temperature in the CP raw model output compared to the coarser 7 km grid with parametrized convection. The improvement found is largest in the summer, where the cold bias in the coarser simulation was substantially reduced. This applies to both the median temperature and the more extreme percentiles (10th and 90th) of the temperature distribution over the model domain in the historical period. The found improvement of the temperature output on the convection permitting scale, confirms the findings by Hackenbruch et al. (2016), Hohenegger et al. (2008), and

475   Laube (2019). However, recent studies have shown that this temperature bias, especially in daily minimum and maximum, can still be addressed in CCLM with an improved formulation of the 2 m temperature in the land surface scheme (Schulz and Vogel, 2020). Moreover, it needs to be clarified whether the improved temperature output in convection permitting simulation justifies the higher computational cost for high-resolution simulations. While systematic biases between raw model temperature output and observations remain in our CPM ensemble, we show a clear benefit from a relatively large simulation area across different

480   landscapes. We find a dependency of the remaining error on the landscape type and an association with orography – especially in transition areas between different major landscape types. Therefore we support a region-specific magnitude of the added value as in Soares et al. (2022). In order to provide information for climate change impact studies or user-oriented studies, in this case focusing on heat stress, there is still a need for bias correction. Especially for threshold-based parameters, bias correction is a necessity to obtain meaningful values. Nevertheless, we expect that such studies will benefit from the better

485   representation of high temperatures on the convection permitting scale due to the smaller impact of bias correction and thus a smaller source of error.

The analysis allows for the first time a very high resolution projection of temperature and temperature extremes over Germany in a 2 and 3 degree warmer world. The regional, high resolution analysis confirms general warming over the whole region and a slightly higher change signal in mountainous regions. As in Vautard et al. (2014), the smallest temperature increase was

490   found in spring. Indeed, the peak of summer temperatures in a warmer climate shifts to later in the summer. Moreover, the analysis confirms a wider distribution of temperature with global warming, implying a greater change of extreme temperature compared to the average warming in the future (e.g. Mearns et al. (1984); Schär et al. (2004); Giorgi et al. (2004); Kjellström et al. (2007); Vidale et al. (2007); IPCC (2021)). Our study shows, that HW probability is expected to increase significantly over Germany and especially in late summer large HWs are anticipated. HW severity is projected to rise dramatically, indicated

495   by a 26 % (100 %) percent increase from 1971-2000 to a 2° (3°) warmer world. Increasing variability in HW characteristics is projected for the future. This is consistent with past trends of HW temperature and duration derived from observational data (Della-Marta et al., 2007). Our study thus suggests that the trend is likely to continue in the future.

Apart from meteorological insights, a closer look at human heat stress and other tailored climate parameters shows the potential of using convection permitting simulations in different fields of application and highlights the importance of individual

500   consideration. Strong human heat stress – parameterized via UTCI>32° as well as associated with very hot days or tropical nights – is prevalent in the flat regions such as the Rhine Valley. Moreover, the largest absolute increase is expected for these regions, comparable to Brecht et al. (2020). The change signal of tailored climate parameters does not always scale linearly with global warming – as is the case for the relative quantity dry hot summers or growing days, a quantity that targets for moderate conditions. Especially for extreme heat stress (UTCI>32°, very hot days, or tropical nights) we see a non-linear

505 but rather exponential increase with global warming. In particular for specialized applications – expressed e.g. over more complex climate parameters – behaviour depends crucially on the prevailing landscape and might even lead to opposing trends. Therefore, the analysis supports previous results of spatial patterns (Schipper et al., 2019; Brecht et al., 2020) and shows the benefit of CPM, which allows the representation of distinct characteristics in clearly defined areas.

Limitations of the study are that the assessment of uncertainty is restricted with four GCMs and only one RCM. However,
510 the magnitude of the uncertainty associated with the RCM choice is typically smaller than from the large-scale GCM forcing (Kjellström et al., 2011). In the future, larger ensembles on the convection permitting scales are expected to be available, enabling assessment of GCM- and RCM-uncertainty. Currently, ongoing downscaling of the CMIP6 GCMs is a promising source of future driving data for high-resolution climate simulations. In particular, the improved representation of northern hemisphere blocking in the new generation of climate models (Schiemann et al., 2020) will necessitate additional analysis
515 of HWs and is anticipated to provide complementary insights to the results shown. Moreover, long convection permitting projections would profit from the implementation of variable land surface characteristics over time, as e.g. recently provided by FPS-LUCAS (Hoffmann et al., 2021). Moving from constant to variable input fields could yield valuable information for heat stress in impact studies. Especially for climate adaptation studies, development is still anticipated for urban areas and the evaluation of according urban parametrization schemes. Since no parametrization is used in this study, further improvements
520 for urban areas are to be expected (e.g. Trusilova et al., 2016; Daniel et al., 2019).

Heat extremes and related impacts derived from a convection permitting ensemble document that the climate change signal depends on major landscape regions. Therefore, such convection permitting projections have the potential to facilitate tailored impact studies and can help to narrow down the gap between climate research and the requirements of stakeholders e.g. for sustainable risk management and climate adaptation. This presented finding stresses the need of climate adaptation strategies
525 on a local level and supports the regional approach in climate adaptation research e.g. in the BMBF RegIKlim project: basic research is done in a pilot region, concentrating on region-specific key issues to develop, evaluate, communicate, and test the implementation of adaptation strategies with the aim of an up-scaling in the concerning region in the future.

Data availability. The ensemble simulation data can be requested from the authors. It is planned to provide parts via the German Climate Computing Center (DKRZ). The observation dataset HYRAS is a product of the Deutscher Wetterdienst DWD. It can be requested at DWD
530 for research purposes

Author contributions. The concept of the paper was developed by MH, HF and JGP. NL performed preliminary analysis. MH is responsible for data analysis and figures. The initial draft was written by MH, supported by HF and JGP. All authors contributed to discussions, comments, and revisions.

Competing interests. The coauthor JGP is a member of the editorial board of Natural Hazards and Earth System Sciences.

535   *Acknowledgements.* The work was conducted within the funding measure „Regional information for action on climate change" (RegIKlim) of the German Federal Ministry of Education and Research (BMBF) in the ISAP project (01LR2007B) and NUKLEUS project (01LR2002B). The study was carried out in cooperation with the project climXtreme – also supported by the BMBF – at KIT (01LP1901A). We thank Hans-Jürgen Panitz and Regina Kohlhepp (KIT/IMK) for their help in the RCM simulations and Ting-Chen Chen (KIT/IMK) for comments and language check. The simulations were performed on the national supercomputers Cray XC40 Hazel Hen and HPE Apollo Hawk at the

540   High Performance Computing Center Stuttgart (HLRS) under the grant number HRCM (ID 12801). Parts of the processing and analysis were performed at DKRZ. We thank the Deutscher Wetterdienst (DWD) for providing observational data. Finally, we thank the open-access publishing fund of KIT.

References

Alexander, L. V., Zhang, X., Peterson, T. C., Caesar, J., Gleason, B., Klein Tank, A., Haylock, M., Collins, D., Trewin, B., Rahimzadeh, F., et al.: Global observed changes in daily climate extremes of temperature and precipitation, J. Geophys. Res. Atmos., 111, https://doi.org/10.1029/2005JD006290, 2006.

Baldauf, M., Seifert, A., Förstner, J., Majewski, D., Raschendorfer, M., and Reinhardt, T.: Operational Convective-Scale Numerical Weather Prediction with the COSMO Model: Description and Sensitivities, Mon. Weather Rev., 139, 3887 – 3905, https://doi.org/10.1175/MWR-D-10-05013.1, 2011.

Ban, N., Schmidli, J., and Schär, C.: Evaluation of the convection-resolving regional climate modeling approach in decade-long simulations, J. Geophys. Res. Atmos., 119, 7889–7907, https://doi.org/10.1002/2014JD021478, 2014.

Ban, N., Caillaud, C., Coppola, E., Pichelli, E., Sobolowski, S., Adinolfi, M., Ahrens, B., Alias, A., Anders, I., Bastin, S., et al.: The first multi-model ensemble of regional climate simulations at kilometer-scale resolution, part I: evaluation of precipitation, Clim. Dynam., 57, 275–302, https://doi.org/10.1007/s00382-021-05708-w, 2021.

Barriopedro, D., Fischer, E. M., Luterbacher, J., Trigo, R. M., and García-Herrera, R.: The hot summer of 2010: redrawing the temperature record map of Europe, Science, 332, 220–224, https://doi.org/10.1126/science.1201224, 2011.

Basu, R. and Samet, J. M.: Relation between elevated ambient temperature and mortality: a review of the epidemiologic evidence., Epidemiol. Rev., 24, 190–202, https://doi.org/10.1093/epirev/mxf007, 2002.

Becker, F., Fink, A., Bissolli, P., and Pinto, J. G.: Towards a more comprehensive assessment of the intensity of historical European heat waves (1979–2019), Atmos. Sci. Let., 23, e1120, https://doi.org/10.1002/asl.1120, 2022.

Berg, P., Feldmann, H., and Panitz, H.-J.: Bias correction of high resolution regional climate model data, J. Hydrol., 448, 80–92, https://doi.org/10.1016/j.jhydrol.2012.04.026, 2012.

Biesbroek, G. R., Swart, R. J., Carter, T. R., Cowan, C., Henrichs, T., Mela, H., Morecroft, M. D., and Rey, D.: Europe adapts to climate change: comparing national adaptation strategies, Global Environmental Change, 20, 440–450, https://doi.org/10.1016/j.gloenvcha.2010.03.005, 2010.

Błażejczyk, K., Jendritzky, G., Bröde, P., Fiala, D., Havenith, G., Epstein, Y., Psikuta, A., and Kampmann, B.: An introduction to the universal thermal climate index (UTCI), Geographia Polonica, 86, 5–10, https://doi.org/http://doi.org./10.7163/GPol.2013.1, 2013.

Brands, S.: A circulation-based performance atlas of the CMIP5 and 6 models for regional climate studies in the Northern Hemisphere mid-to-high latitudes, Geosci. Model Dev., 15, 1375–1411, https://doi.org/10.5194/gmd-15-1375-2022, 2022.

Brecht, B. M., Schädler, G., and Schipper, J. W.: UTCI climatology and its future change in Germany–an RCM ensemble approach, Meteorol. Z., 29, 97–116, https://doi.org/0.1127/metz/2020/1010, 2020.

Brisson, E., Van Weverberg, K., Demuzere, M., Devis, A., Saeed, S., Stengel, M., and van Lipzig, N. P.: How well can a convection-permitting climate model reproduce decadal statistics of precipitation, temperature and cloud characteristics?, Clim. Dynam., 47, 3043–3061, https://doi.org/10.1007/s00382-016-3012-z, 2016.

Cannon, A. J., Sobie, S. R., and Murdock, T. Q.: Bias correction of GCM precipitation by quantile mapping: how well do methods preserve changes in quantiles and extremes?, Journal of Climate, 28, 6938–6959, https://doi.org/10.1175/JCLI-D-14-00754.1, 2015.

Collins, W., Bellouin, N., Doutriaux-Boucher, M., Gedney, N., Halloran, P., Hinton, T., Hughes, J., Jones, C., Joshi, M., Liddicoat, S., et al.: Development and evaluation of an Earth-System model–HadGEM2, Geosci. Model Dev., 4, 1051–1075, https://doi.org/10.5194/gmd-4-1051-2011, 2011.

580   Daniel, M., Lemonsu, A., Déqué, M., Somot, S., Alias, A., and Masson, V.: Benefits of explicit urban parameterization in regional climate modeling to study climate and city interactions, Clim. Dynam., 52, 2745–2764, https://doi.org/10.1007/s00382-018-4289-x, 2019.

De Bono, A., Peduzzi, P., Kluser, S., and Giuliani, G.: Impacts of summer 2003 heat wave in Europe, Environment Alert Bulletin, 2, 4, https://archive-ouverte.unige.ch/unige:32255, 2004.

Della-Marta, P. M., Haylock, M. R., Luterbacher, J., and Wanner, H.: Doubled length of western European summer heat waves since 1880,

585   J. Geophys. Res. Atmos., 112, https://doi.org/10.1029/2007JD008510, 2007.

Ehmele, F., Kautz, L.-A., Feldmann, H., He, Y., Kadlec, M., Kelemen, F. D., Lentink, H. S., Ludwig, P., Manful, D., and Pinto, J. G.: Adaptation and application of the large LAERTES-EU regional climate model ensemble for modeling hydrological extremes: a pilot study for the Rhine basin, Nat. Hazards Earth Syst. Sci., 22, 677–692, https://doi.org/10.5194/nhess-22-677-2022, 2022.

Fanger, P. O.: Thermal comfort. Analysis and applications in environmental engineering., Copenhagen: Danish Technical Press.,

590   https://doi.org/10.1177/146642407209200337, 1970.

Fiala, D., Havenith, G., Bröde, P., Kampmann, B., and Jendritzky, G.: UTCI-Fiala multi-node model of human heat transfer and temperature regulation, Int. J. Biometeorol., 56, 429–441, https://doi.org/10.1007/s00484-011-0424-7, 2012.

García-Herrera, R., Díaz, J., Trigo, R. M., Luterbacher, J., and Fischer, E. M.: A review of the European summer heat wave of 2003, Crit. Rev. Env. Sci. Tech., 40, 267–306, https://doi.org/10.1080/10643380802238137, 2010.

595   Giorgetta, M. A., Jungclaus, J., Reick, C. H., Legutke, S., Bader, J., Böttinger, M., Brovkin, V., Crueger, T., Esch, M., Fieg, K., et al.: Climate and carbon cycle changes from 1850 to 2100 in MPI-ESM simulations for the Coupled Model Intercomparison Project phase 5, J. Adv. Model. Earth Sy., 5, 572–597, https://doi.org/10.1002/jame.20038, 2013.

Giorgi, F., Bi, X., and Pal, J.: Mean, interannual variability and trends in a regional climate change experiment over Europe. II: climate change scenarios (2071–2100), Clim. Dynam., 23, 839–858, https://doi.org/10.1007/s00382-004-0467-0, 2004.

600   Hackenbruch, J., Schädler, G., and Schipper, J. W.: Added value of high-resolution regional climate simulations for regional impact studies, Meteorol. Z., 25, 291–304, https://doi.org/10.1127/metz/2016/0701, 2016.

Hackenbruch, J., Kunz-Plapp, T., Müller, S., and Schipper, J. W.: Tailoring climate parameters to information needs for local adaptation to climate change, Climate, 5, 25, https://doi.org/10.3390/cli5020025, 2017.

Havenith, G., Fiala, D., Błazejczyk, K., Richards, M., Bröde, P., Holmér, I., Rintamaki, H., Benshabat, Y., and Jendritzky, G.: The UTCI-

605   clothing model, Int. J. Biometeorol., 56, 461–470, https://doi.org/10.1007/s00484-011-0451-4, 2012.

Hoffmann, P., Reinhart, V., Rechid, D., de Noblet-Ducoudré, N., Davin, E. L., Asmus, C., Bechtel, B., Böhner, J., Katragkou, E., and Luyssaert, S.: High-resolution land-use land-cover change data for regional climate modelling applications over Europe–Part 2: Historical and future changes, Earth Syst. Sci. Data Discussions, pp. 1–43, https://doi.org/10.5194/essd-2021-252, 2021.

Hohenegger, C., Brockhaus, P., and Schar, C.: Towards climate simulations at cloud-resolving scales, Meteorol. Z., 17, 383–394,

610   https://doi.org/10.1127/0941-2948/2008/0303, 2008.

IPCC: Climate Change 2021: The Physical Science Basis. Contribution of Working Group I to the Sixth Assessment Report of the Intergovernmental Panel on Climate Change, vol. In Press, Cambridge University Press, Cambridge, United Kingdom and New York, NY, USA, https://doi.org/10.1017/9781009157896, 2021.

Jacob, D., Petersen, J., Eggert, B., Alias, A., Christensen, O. B., Bouwer, L. M., Braun, A., Colette, A., Déqué, M., Georgievski, G., et al.:

615   EURO-CORDEX: new high-resolution climate change projections for European impact research, Reg. Environ. Change, 14, 563–578, https://doi.org/10.1007/s10113-013-0499-2, 2014.

Jendritzky, G., Havenith, G., Weihs, P., Batchvarova, E., and DeDear, R.: The universal thermal climate index UTCI goal and state of COST action 730, in: 18th International Conference on Biometeorology, Tokyo, 2008.

Jendritzky, G., de Dear, R., and Havenith, G.: UTCI—why another thermal index?, Int. J. Biometeorol., 56, 421–428, https://doi.org/10.1007/s00484-011-0513-7, 2012.

Kerkhoff, C., Künsch, H. R., and Schär, C.: Assessment of bias assumptions for climate models, Journal of Climate, 27, 6799–6818, https://doi.org/10.1175/JCLI-D-13-00716.1, 2014.

Kjellström, E., Bärring, L., Jacob, D., Jones, R., Lenderink, G., and Schär, C.: Modelling daily temperature extremes: recent climate and future changes over Europe, Climatic Change, 81, 249–265, https://doi.org/10.1007/s10584-006-9220-5, 2007.

Kjellström, E., Nikulin, G., Hansson, U., Strandberg, G., and Ullerstig, A.: 21st century changes in the European climate: uncertainties derived from an ensemble of regional climate model simulations, Tellus A, 63, 24–40, https://doi.org/10.1111/j.1600-0870.2010.00475.x, 2011.

Kyselỳ, J.: Influence of the persistence of circulation patterns on warm and cold temperature anomalies in Europe: analysis over the 20th century, Global and Planetary change, 62, 147–163, https://doi.org/10.1016/j.gloplacha.2008.01.003, 2008.

Laube, N.: Predictability of European Heat Waves, Ph.D. thesis, Karlsruher Institut für Technologie (KIT), https://doi.org/10.5445/IR/1000098837, 2019.

Lavin-Gullon, A., Milovac, J., Garcia-Diez, M., and Fernandez, J.: Spin-up time and internal variability analysis for overlapping time slices in a regional climate model, Clim. Dynam., https://doi.org/10.1007/s00382-022-06560-2, 2022.

Lee, J.-Y., Marotzke, J., Bala, G., Cao, L., Corti, S., Dunne, J., Engelbrecht, F., Fischer, E., Fyfe, J., Jones, C., Maycock, A., Mutemi, J., Ndiaye, O., Panickal, S., and Zhou, T.: Future Global Climate: Scenario-Based Projections and Near-Term Information, p. 553–672, Cambridge University Press, Cambridge, United Kingdom and New York, NY, USA, https://doi.org/10.1017/9781009157896.006, 2021.

Lee, T. M., Markowitz, E. M., Howe, P. D., Ko, C.-Y., and Leiserowitz, A. A.: Predictors of public climate change awareness and risk perception around the world, Nat. Clim. Change, 5, 1014–1020, https://doi.org/10.1038/nclimate2728, 2015.

Lemos, M. C., Kirchhoff, C. J., and Ramprasad, V.: Narrowing the climate information usability gap, Nat. Clim. Change, 2, 789–794, https://doi.org/10.1038/nclimate1614, 2012.

Maraun, D.: Bias correcting climate change simulations-a critical review, Current Climate Change Reports, 2, 211–220, https://doi.org/10.1007/s40641-016-0050-x, 2016.

Mearns, L. O., Katz, R. W., and Schneider, S. H.: Extreme high-temperature events: changes in their probabilities with changes in mean temperature, J. Appl. Meteorol. Clim., 23, 1601–1613, https://doi.org/10.1175/1520-0450(1984)023<1601:EHTECI>2.0.CO;2, 1984.

Moser, S. C.: Reflections on climate change communication research and practice in the second decade of the 21st century: what more is there to say?, Wires. Clim. Change, 7, 345–369, https://doi.org/10.1002/wcc.403, 2016.

Nairn, J. R. and Fawcett, R. J.: The excess heat factor: a metric for heatwave intensity and its use in classifying heatwave severity, Int. J. Env. Res. Pub. He., 12, 227–253, https://doi.org/10.3390/ijerph120100227, 2015.

Nijsse, F. J., Cox, P. M., and Williamson, M. S.: Emergent constraints on transient climate response (TCR) and equilibrium climate sensitivity (ECS) from historical warming in CMIP5 and CMIP6 models, Earth Syst. Dynam., 11, 737–750, https://doi.org/10.5194/esd-11-737-2020, 2020.

Pastén-Zapata, E., Jones, J. M., Moggridge, H., and Widmann, M.: Evaluation of the performance of Euro-CORDEX Regional Climate Models for assessing hydrological climate change impacts in Great Britain: A comparison of different spatial resolutions and quantile mapping bias correction methods, Journal of Hydrology, 584, 124 653, https://doi.org/10.1016/j.jhydrol.2020.124653, 2020.

Perez, J., Menendez, M., Mendez, F. J., and Losada, I. J.: Evaluating the performance of CMIP3 and CMIP5 global climate models over the north-east Atlantic region, Clim. Dynam., 43, 2663–2680, https://doi.org/10.1007/s00382-014-2078-8, 2014.

Perkins, S. E. and Alexander, L. V.: On the measurement of heat waves, J. Climate, 26, 4500–4517, https://doi.org/10.1175/JCLI-D-12-00383.1, 2013.

Pichelli, E., Coppola, E., Sobolowski, S., Ban, N., Giorgi, F., Stocchi, P., Alias, A., Belušić, D., Berthou, S., Caillaud, C., et al.: The first multi-model ensemble of regional climate simulations at kilometer-scale resolution part 2: historical and future simulations of precipitation, Clim. Dynam., 56, 3581–3602, https://doi.org/10.1007/s00382-021-05657-4, 2021.

Pierce, D. W., Cayan, D. R., Maurer, E. P., Abatzoglou, J. T., and Hegewisch, K. C.: Improved bias correction techniques for hydrological simulations of climate change, Journal of Hydrometeorology, 16, 2421–2442, https://doi.org/10.1175/JHM-D-14-0236.1, 2015.

Poumadere, M., Mays, C., Le Mer, S., and Blong, R.: The 2003 heat wave in France: dangerous climate change here and now, Risk Anal., 25, 1483–1494, https://doi.org/10.1111/j.1539-6924.2005.00694.x, 2005.

Prein, A., Gobiet, A., Suklitsch, M., Truhetz, H., Awan, N., Keuler, K., and Georgievski, G.: Added value of convection permitting seasonal simulations, Clim. Dynam., 41, 2655–2677, https://doi.org/10.1007/s00382-013-1744-6, 2013.

Prein, A. F., Langhans, W., Fosser, G., Ferrone, A., Ban, N., Goergen, K., Keller, M., Tölle, M., Gutjahr, O., Feser, F., et al.: A review on regional convection-permitting climate modeling: Demonstrations, prospects, and challenges, Rev. Geophys., 53, 323–361, https://doi.org/10.1002/2014RG000475, 2015.

Prodhomme, C., Doblas-Reyes, F., Bellprat, O., and Dutra, E.: Impact of land-surface initialization on sub-seasonal to seasonal forecasts over Europe, Clim. Dynam., 47, 919–935, https://doi.org/10.1007/s00382-015-2879-4, 2016.

Qian, W. and Chang, H. H.: Projecting Health Impacts of Future Temperature: A Comparison of Quantile-Mapping Bias-Correction Methods, Int. J. Env. Res. Pub. He., 18, 1992, https://doi.org/10.3390/ijerph18041992, 2021.

Rauthe, M., Steiner, H., Riediger, U., Mazurkiewicz, A., and Gratzki, A.: A Central European precipitation climatology–Part I: Generation and validation of a high-resolution gridded daily data set (HYRAS), Meteorol. Z., 22, 235–256, https://doi.org/10.1127/0941-2948/2013/0436, 2013.

Razafimaharo, C., Krähenmann, S., Höpp, S., Rauthe, M., and Deutschländer, T.: New high-resolution gridded dataset of daily mean, minimum, and maximum temperature and relative humidity for Central Europe (HYRAS), Theor. Appl. Climatol., 142, 1531–1553, https://doi.org/10.1007/s00704-020-03388-w, 2020.

Reckien, D., Salvia, M., Heidrich, O., Church, J. M., Pietrapertosa, F., de Gregorio-Hurtado, S., d'Alonzo, V., Foley, A., Simoes, S. G., Lorencová, E. K., et al.: How are cities planning to respond to climate change? Assessment of local climate plans from 885 cities in the EU-28, J. Clean. Prod., 191, 207–219, https://doi.org/10.1016/j.jclepro.2018.03.220, 2018.

Robine, J.-M., Cheung, S. L., Le Roy, S., Van Oyen, H., and Herrmann, F. R.: Report on excess mortality in Europe during summer 2003, EU Community Action Programme for Public Health, Grant Agreement, 2005114, 28, 2007.

Rockel, B., Will, A., and Hense, A.: The regional climate model COSMO-CLM (CCLM), Meteorol. Z., 17, 347–348, https://doi.org/0.1127/0941-2948/2008/0309, 2008.

Russo, S., Dosio, A., Graversen, R. G., Sillmann, J., Carrao, H., Dunbar, M. B., Singleton, A., Montagna, P., Barbola, P., and Vogt, J. V.: Magnitude of extreme heat waves in present climate and their projection in a warming world, J. Geophys. Res. Atmos., 119, 12–500, https://doi.org/10.1002/2014JD022098, 2014.

Russo, S., Sillmann, J., and Fischer, E. M.: Top ten European heatwaves since 1950 and their occurrence in the coming decades, Environ. Res. Lett., 10, 124 003, https://doi.org/http://doi.org/10.1088/1748-9326/10/12/124003, 2015.

Schädler, G., Panitz, H.-J., Christner, E., Feldmann, H., Karremann, M., and Laube, N.: Regional Climate Simulations with COSMO-CLM: Ensembles, Very High Resolution and Paleoclimate, in: High Performance Computing in Science and Engineering'17, pp. 411–429, Springer, https://doi.org/10.1007/978-3-319-68394-2_24, 2018.

Schär, C. and Jendritzky, G.: Hot news from summer 2003, Nature, 432, 559–560, https://doi.org/10.1038/432559a, 2004.

Schär, C., Vidale, P. L., Lüthi, D., Frei, C., Häberli, C., Liniger, M. A., and Appenzeller, C.: The role of increasing temperature variability in European summer heatwaves, Nature, 427, 332–336, https://doi.org/10.1038/nature02300, 2004.

Schiemann, R., Athanasiadis, P., Barriopedro, D., Doblas-Reyes, F., Lohmann, K., Roberts, M. J., Sein, D. V., Roberts, C. D., Terray, L., and Vidale, P. L.: Northern Hemisphere blocking simulation in current climate models: evaluating progress from the Climate Model Intercomparison Project Phase 5 to 6 and sensitivity to resolution, Weather Clim. Dyn., 1, 277–292, https://doi.org/10.5194/wcd-1-277-2020, 2020.

Schipper, J., Hackenbruch, J., Lentink, H., Nerding, K.-U., and Müller, S.: Sensitivitätsbereiche von branchenspezifischen Klimakenngrößen in Baden-Württemberg – die „Sensitivitätsampel", KLIMOPASS-Berichte, https://pd.lubw.de/30392, 2016.

Schipper, J. W., Hackenbruch, J., Lentink, H. S., and Sedlmeier, K.: Integrating Adaptation Expertise into Regional Climate Data Analyses through Tailored Climate Parameters, Meteorol. Z., pp. 41–57, https://doi.org/10.1127/metz/2019/0878, 2019.

Schrodin, R. and Heise, E.: The Multi-Layer Version of the DWD Soil Model TERRA-LM, COSMO Technical Report, https://doi.org/0.5676/DWD_pub/nwv/cosmo-tr_2, 2001.

Schubert, D., van der Linden, R., Fink, A. H., Katzfey, J., Phan-Van, T., Maßmeyer, K., and Pinto, J. G.: Klimaprojektionen für die hydrologische Modellierung in Südvietnam, Hydrologie und Wasserbewirtschaftung, 61, 383–396, https://doi.org/10.5675/HyWa_2017,6_2, 2017.

Schulz, J.-P. and Vogel, G.: Improving the processes in the land surface scheme TERRA: Bare soil evaporation and skin temperature, Atmosphere, 11, 513, https://doi.org/10.3390/atmos11050513, 2020.

Soares, P., Careto, J., Cardoso, R. M., Goergen, K., Katragkou, E., Sobolowski, S., Coppola, E., Ban, N., Belušić, D., Berthou, S., Caillaud, C., Dobler, A., Hodnebrog, O., Kartsios, S., Lenderink, G., Lorenz, T., Milovac, J., Feldmann, H., Pichelli, E., Truhetz, H., Demory, M., de Vries, H., Warrach-Sagi, K., Keuler, K., Raffa, M., and Tölle, M. Sieck, K. B. S.: The added value of km-scale simulations to describe temperature over complex orography: the CORDEX FPS-Convection multi-model ensemble runs over the Alps, Clim. Dynam. Preprint, https://doi.org/10.5194/gmd-14-5125-2021, 2022.

Sørland, S. L., Brogli, R., Pothapakula, P. K., Russo, E., Van de Walle, J., Ahrens, B., Anders, I., Bucchignani, E., Davin, E. L., Demory, M.-E., et al.: COSMO-CLM regional climate simulations in the Coordinated Regional Climate Downscaling Experiment (CORDEX) framework: a review, Geosci. Model Dev., 14, 5125–5154, https://doi.org/10.5194/gmd-14-5125-2021, 2021.

Taylor, K. E., Stouffer, R. J., and Meehl, G. A.: An overview of CMIP5 and the experiment design, B. Am. Meteorol. Soc., 93, 485–498, https://doi.org/10.1175/BAMS-D-11-00094.1, 2012.

Teichmann, C., Bülow, K., Otto, J., Pfeifer, S., Rechid, D., Sieck, K., and Jacob, D.: Avoiding extremes: Benefits of staying below +1.5 C compared to +2.0 C and +3.0 C global warming, Atmosphere, 9, 115, https://doi.org/10.3390/atmos9040115, 2018.

Tiedtke, M.: A comprehensive mass flux scheme for cumulus parameterization in large-scale models, Mon. Weather Rev., 117, 1779–1800, https://doi.org/10.1175/1520-0493(1989)117<1779:ACMFSF>2.0.CO;2, 1989.

Tölle, M. H., Schefczyk, L., and Gutjahr, O.: Scale dependency of regional climate modeling of current and future climate extremes in Germany, Theor. Appl. Climatology, 134, 829–848, https://doi.org/10.1007/s00704-017-2303-6, 2018.

Trusilova, K., Schubert, S., Wouters, H., Früh, B., Grossman-Clarke, S., Demuzere, M., and Becker, P.: The urban land use in the COSMO-CLM model: a comparison of three parameterizations for Berlin, Meteorol. Z., 25, 231–244, https://doi.org/10.1127/metz/2015/0587, 2016.

Uppala, S. M., KÅllberg, P. W., Simmons, A. J., Andrae, U., Bechtold, V. D. C., Fiorino, M., Gibson, J. K., Haseler, J., Hernandez, A., Kelly, G. A., Li, X., Onogi, K., Saarinen, S., Sokka, N., Allan, R. P., Andersson, E., Arpe, K., Balmaseda, M. A., Beljaars, A. C. M., Berg, L. V. D., Bidlot, J., Bormann, N., Caires, S., Chevallier, F., Dethof, A., Dragosavac, M., Fisher, M., Fuentes, M., Hagemann, S., Hólm, E., Hoskins, B. J., Isaksen, L., Janssen, P. A. E. M., Jenne, R., Mcnally, A. P., Mahfouf, J.-F., Morcrette, J.-J., Rayner, N. A., Saunders, R. W., Simon, P., Sterl, A., Trenberth, K. E., Untch, A., Vasiljevic, D., Viterbo, P., and Woollen, J.: The ERA-40 re-analysis, Q. J. Roy. Meteor. Soc., 131, 2961–3012, https://doi.org/https://doi.org/10.1256/qj.04.176, 2005.

Van Vuuren, D. P., Edmonds, J., Kainuma, M., Riahi, K., Thomson, A., Hibbard, K., Hurtt, G. C., Kram, T., Krey, V., Lamarque, J.-F., et al.: The representative concentration pathways: an overview, Climatic change, 109, 5–31, https://doi.org/10.1007/s10584-011-0148-z, 2011.

Vautard, R., Gobiet, A., Sobolowski, S., Kjellström, E., Stegehuis, A., Watkiss, P., Mendlik, T., Landgren, O., Nikulin, G., Teichmann, C., et al.: The European climate under a 2° C global warming, Environ. Res. Lett., 9, 034 006, https://doi.org/10.1088/1748-9326/9/3/034006, 2014.

Vidale, P. L., Lüthi, D., Wegmann, R., and Schär, C.: European summer climate variability in a heterogeneous multi-model ensemble, Climatic Change, 81, 209–232, https://doi.org/10.1007/s10584-006-9218-z, 2007.

Voldoire, A., Sanchez-Gomez, E., Salas y Mélia, D., Decharme, B., Cassou, C., Sénési, S., Valcke, S., Beau, I., Alias, A., Chevallier, M., et al.: The CNRM-CM5. 1 global climate model: description and basic evaluation, Clim. Dynam., 40, 2091–2121, https://doi.org/10.1007/s00382-011-1259-y, 2013.

Vrac, M. and Naveau, P.: Stochastic downscaling of precipitation: From dry events to heavy rainfalls, Water resources research, 43, https://doi.org/10.1029/2006WR005308, 2007.

Zuo, J., Pullen, S., Palmer, J., Bennetts, H., Chileshe, N., and Ma, T.: Impacts of heat waves and corresponding measures: a review, J. Clean. Prod., 92, 1–12, https://doi.org/10.1016/j.jclepro.2014.12.078, 2015.